Article

Immunity

Single-cell and spatial transcriptomics reveal aberrant lymphoid developmental programs driving granuloma formation

Graphical abstract

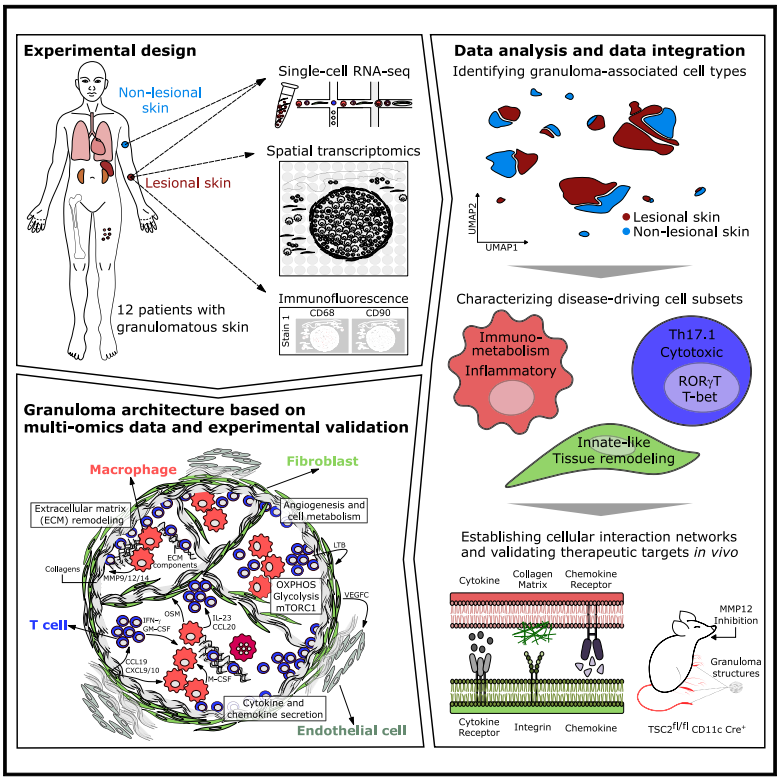

Highlights

- Performed single-cell sequencing and spatial transcriptomics on sarcoidosis granulomas
- Reconstructed the architecture of granulomas and their gene regulatory networks
- Identified a network of pathogenic macrophages, T cells, and fibroblasts in granulomas
- Tested mechanisms shared with lymphoid organ development as drug targets in sarcoidosis

Authors

Thomas Krausgruber, Anna Redl, Daniele Barreca, ..., Thomas Weichhart, Christoph Bock, Georg Stary

Correspondence

cbock@cemm.oeaw.ac.at (C.B.), georg.stary@meduniwien.ac.at (G.S.)

In brief

Granulomas are accumulations of immune cells that help contain infections but can also give rise to diseases. To better understand granuloma formation, Krausgruber et al. perform single-cell and spatial profiling of sarcoidosis-associated skin granulomas. They find that granulomas exploit molecular mechanisms underlying the formation of tertiary lymphoid structures but lack their overall control, indicating that granulomas constitute aberrant lymphoid organs.

Krausgruber et al., 2023, Immunity *56*, 289–306
February 14, 2023
https://doi.org/10.1016/j.immuni.2023.01.014

CellPress

Immunity

CellPress
OPEN ACCESS

Article

Single-cell and spatial transcriptomics reveal aberrant lymphoid developmental programs driving granuloma formation

Thomas Krausgruber,[1,2,7] Anna Redl,[1,3,7] Daniele Barreca,[1,7] Konstantin Doberer,[4] Daria Romanovskaia,[1] Lina Dobnikar,[1] Maria Guarini,[1] Luisa Unterluggauer,[3] Lisa Kleissl,[3,5] Denise Atzmüller,[5] Carolina Mayerhofer,[3] Aglaja Kopf,[1,3,5] Simona Saluzzo,[3] Clarice X. Lim,[6] Praveen Rexie,[6] Thomas Weichhart,[6] Christoph Bock,[1,2,5,8,*] and Georg Stary[1,3,5,8,9,*]

[1]CeMM Research Center for Molecular Medicine of the Austrian Academy of Sciences, Vienna, Austria
[2]Medical University of Vienna, Institute of Artificial Intelligence, Center for Medical Data Science, Vienna, Austria
[3]Medical University of Vienna, Department of Dermatology, Vienna, Austria
[4]Medical University of Vienna, Department of Medicine III, Division of Nephrology and Dialysis, Vienna, Austria
[5]Ludwig Boltzmann Institute for Rare and Undiagnosed Diseases, Vienna, Austria
[6]Medical University of Vienna, Institute of Medical Genetics, Center for Pathobiochemistry and Genetics, Vienna, Austria
[7]These authors contributed equally
[8]Senior author
[9]Lead contact
*Correspondence: cbock@cemm.oeaw.ac.at (C.B.), georg.stary@meduniwien.ac.at (G.S.)
https://doi.org/10.1016/j.immuni.2023.01.014

SUMMARY

Granulomas are lumps of immune cells that can form in various organs. Most granulomas appear unstructured, yet they have some resemblance to lymphoid organs. To better understand granuloma formation, we performed single-cell sequencing and spatial transcriptomics on granulomas from patients with sarcoidosis and bioinformatically reconstructed the underlying gene regulatory networks. We discovered an immune stimulatory environment in granulomas that repurposes transcriptional programs associated with lymphoid organ development. Granuloma formation followed characteristic spatial patterns and involved genes linked to immunometabolism, cytokine and chemokine signaling, and extracellular matrix remodeling. Three cell types emerged as key players in granuloma formation: metabolically reprogrammed macrophages, cytokine-producing Th17.1 cells, and fibroblasts with inflammatory and tissue-remodeling phenotypes. Pharmacological inhibition of one of the identified processes attenuated granuloma formation in a sarcoidosis mouse model. We show that human granulomas adopt characteristic aspects of normal lymphoid organ development in aberrant combinations, indicating that granulomas constitute aberrant lymphoid organs.

INTRODUCTION

Granulomas form in response to infections by bacteria and fungi, but they also contribute to diseases such as sarcoidosis, berylliosis, and rheumatoid arthritis.[1,2] Granulomas can cause fibrosis and organ damage, resulting in major disease burden.[3–6] While granuloma formation is an evolutionary adaptive process that helps the immune system contain certain infections or foreign objects in the body, granulomatous inflammation can also emerge without a known initial trigger.[7,8]

Granulomas are complex structures that comprise innate and adaptive immune cells as well as structural cells including fibroblasts and endothelial cells.[2] Their cellular composition is similar across granulomatous disorders, while the microanatomic distribution of these cells and their cytokine profile differ widely. Macrophages are the most common type of immune cell in granulomas. They can become tightly linked and form structures called ''epitheloid cells'' or even fuse into multinucleated giant cells.[9,10] Furthermore, macrophages in granulomas can undergo metabolic dysregulation that results in enhanced inflammation,[11,12] and they often interact with various T cell subtypes such as Th2 cells in granulomas in helminth infections,[13] interferon (IFN)-γ-producing Th1 cells in tuberculosis,[14] as well as Th1 and Th17 cells in Crohn disease.[15] The granuloma border is encompassed by fibroblasts that produce extracellular matrix (ECM) components, contributing to fibrosis and loss of organ function. Recent studies suggest that a network of interactions between immune cells and structural cells helps maintain granulomatous inflammation and organization.[16,17]

To dissect the molecular and cellular processes of granuloma formation, we focused on cutaneous sarcoidosis as a non-infectious granulomatous disease,[18,19] providing a model with no obvious biological justification for or benefit of granuloma formation. Granulomas in sarcoidosis appear to be caused by environmental stimuli,[20–22] dysregulated immune response,[12,23,24] and genetic factors.[25–28] There are few options for targeted

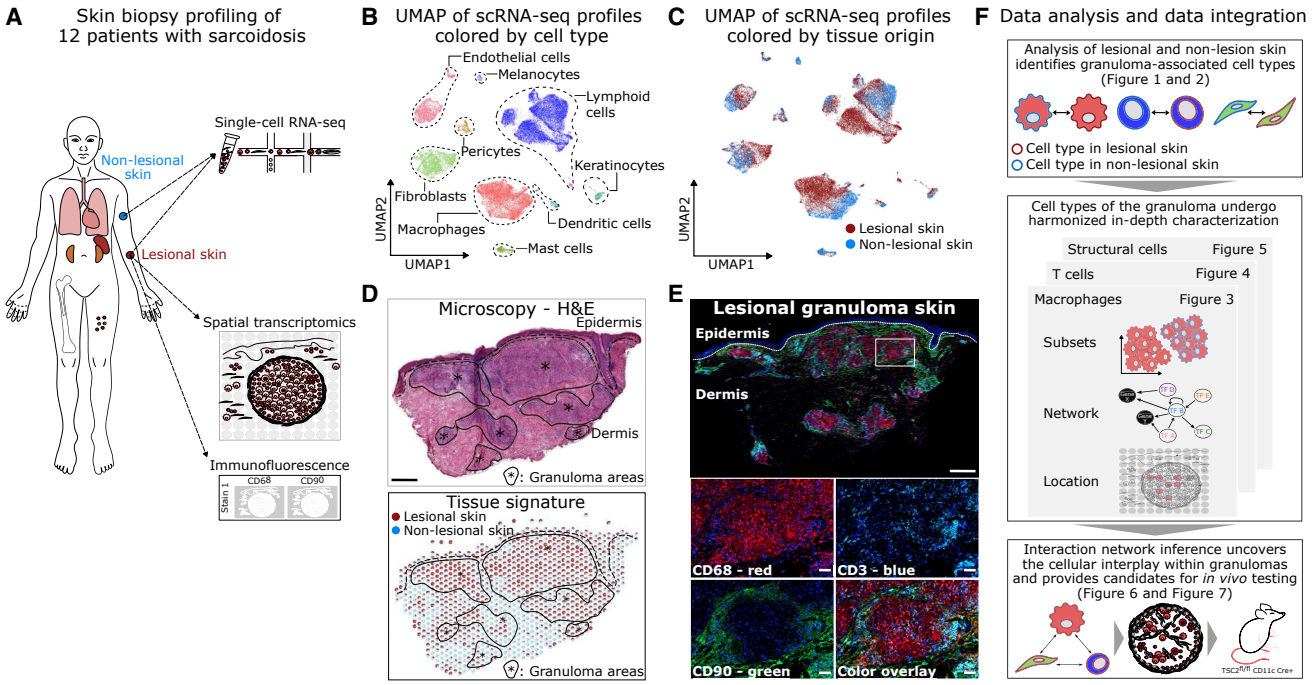

Figure 1. Macrophages, T cells, and fibroblasts are the main cell types in skin granulomas

(A) Schematic of single-cell and spatial profiling for patients with sarcoidosis.

(B) UMAP of scRNA-seq transcriptome profiles from lesional and non-lesional skin. Cells are color-coded according to their assigned cell types based on automated label transfer from a published reference of cell types in healthy skin.[31]

(C) UMAP of scRNA-seq transcriptome profiles color-coded by sample origin.

(D) Spatial transcriptomics data of one representative patient analyzed for lesional and non-lesional tissue signatures. Top: H&E staining of lesional skin; the dotted line indicates the basal membrane between dermis and epidermis; black lines and stars depict the granuloma area. Scale bar: 500 μm. Bottom: proportion of the lesional tissue signature (red) and non-lesional tissue signature (blue) for each spot in the spatial transcriptomics data.

(E) Immunofluorescence protein staining of skin granulomas for the macrophage marker CD68 (red; APC), the T cell marker CD3 (light blue; PE-TR), the fibroblast marker CD90 (green; FITC), and nuclei staining with DAPI (dark blue). Scale bars: 500 μm (main panel) and 50 μm (zoom-in panels).

(F) Schematic of data analysis and data integration strategy. Data in (B) and (C) are from 12 independent patients.

See also Figure S1 and Tables S1 and S2.

therapy, and broad immunosuppressive therapies come with various side effects.[29,30] Sarcoidosis and other granulomatous diseases thus constitute an unmet medical need.

To unravel the gene regulatory programs and cell-cell interactions underlying granuloma formation, we combined single-cell RNA sequencing (scRNA-seq) and spatial transcriptomics with in-depth analysis of cellular marker proteins in granulomas and matched non-lesional skin. For 12 patients with sarcoidosis at baseline of a closely monitored clinical study, we collected scRNA-seq profiles and spatial transcriptomics data. Our analysis of the molecular and cellular architecture of granulomas identified transcriptional programs associated with lymphoid organ development. We specifically investigated granuloma-associated ("GA") macrophages, Th17.1 cells, and fibroblasts, which were interconnected by paracrine cell-cell communication networks inside granulomas. We identified pathomechanisms that were shared across individuals and organs, providing potential targets for therapeutic intervention.

Overall, our study uncovered a mix of developmental programs that underlie granuloma formation, and it highlights the interplay of innate, adaptive, and structural cells in the creation and maintenance of granulomas as a form of aberrant lymphoid organs.

RESULTS

Macrophages, T cells, and fibroblasts are the main cell types in skin granulomas

To study cell composition and gene regulation in granulomas, we performed scRNA-seq on paired biopsies of lesional and non-lesional skin from 12 patients with histologically validated and clinically well-documented persistent cutaneous sarcoidosis (Figure 1A; Table S1). We included 8 female and 4 male patients with a median age of 54 years. Our cohort captures a wide spectrum of skin morphologies, including papules, nodules, plaques, subcutaneous lesions, and tattoo-associated sarcoidosis (Table S1). Overall, ~56,000 single-cell transcriptomes passed quality control (Figure S1A; Table S2; supplemental website: http://granuloma-map.bocklab.org) and were integrated into a joint map, clustered, and subjected to automated cell-type annotation.

We identified eight main cell types shared across patients: lymphoid cells, myeloid cells, keratinocytes, mast cells, fibroblasts, endothelial cells, pericytes, and melanocytes (Figures 1B, S1B, and S1C). We detected widespread transcriptional changes in lesional compared with non-lesional skin (Figure 1C). To confirm that the transcriptional state of cells derived from non-lesional skin

is similar to unperturbed skin, we compared our transcriptional profiles with published data of skin biopsies from healthy donors.[32] We observed consistent clustering of cells from non-lesional skin with healthy control skin, which supports our use of matched non-lesional skin from patients with sarcoidosis as a suitable reference of "normal" skin to which we compared the lesional skin samples (Figures S1D and S1E).

To map the tissue context of the granulomas, we performed spatial transcriptomics and immunofluorescence protein staining of skin biopsies from all 12 patients (Figure 1A; Table S2). We deconvoluted the spatial transcriptomics profiles into regions of lesional and non-lesional skin by using gene signatures derived from our scRNA-seq data (Figures 1D and S1F). Immunofluorescence protein staining identified $CD3^+$ T cells, $CD68^+$ macrophages, and $CD90^+$ fibroblasts as main cell types within granulomas (Figure 1E), confirming and extending our scRNA-seq data analysis (Figures 1B and 1C). Together, these single-cell and spatial maps allowed us to systematically investigate the main cell types in sarcoidosis granulomas and their interplay, using integrative bioinformatic methods (Figure 1F).

Specific macrophage, T cell, and fibroblast cell subsets accumulate in granulomas

We identified 20 cell clusters based on transcriptional similarity, which we labeled according to their expression of known marker genes (Figures 2A and S2A). Seven non-immune (mainly structural cells) clusters and 13 immune cell clusters were observed in lesional and non-lesional skin. The structural cells included blood endothelial cells (characterized by the expression of genes such as *ACKR1*, *PECAM1*, and *VWF*), lymphatic endothelial cells (*PDPN* and *PROX1*), fibroblasts (*THY1* and *FAP*), keratinocytes (*KRT14*), melanocytes (*MLANA*), and smooth muscle cells (*MCAM*). Among the immune cells, we distinguished dendritic cells (*CD1a* and *CD1c*), cytotoxic T cells (*CD3*, *CD8*, and *GZMK*), helper T cells (*CD3* and *CD4*), regulatory T cells (*CD3*, *CD4*, and *IL2RA*), natural killer (NK) cells (*FCGR3A*, *GNLY*, and *GZMK*), B cells (*CD79A* and *IGKC*), macrophages (*CSF1R*, *CD14*, *CD68*, and *CD163*), and mast cells (*KIT* and *TPSAB1*) (Figure 2B).

Cells from cluster 0 (lesional macrophages), cluster 1 (lesional helper T cells), and cluster 9 (lesional fibroblasts) were almost exclusively found in lesional skin. By contrast, endothelial cells, epithelial cells, melanocytes, mast cells, dendritic cells, and certain lymphoid cell subsets showed no such differences (Figure 2C). This indicates that lesional skin is enriched for macrophages, helper T cells, and fibroblasts with a unique transcriptional cell state, but not for other cell types.

To assess the localization of these cell subsets, we performed UMAP dimensionality reduction and unsupervised clustering of the spatial transcriptomics data, resulting in four clusters (Figures 2D and S2B). Cluster 0, 1, and 2 were shared across all samples, whereas cluster 3 contained mainly smooth muscle cells and was restricted to those samples that included vascular tissue (Figure S2C). We histologically annotated these clusters as granulomatous dermis (cluster 0), unaffected dermis (cluster 1), and epidermis (cluster 2) (Figures 2D, 2E, and S2C). Deconvolution of cell-type composition showed that the lesional subsets of macrophages, helper T cells, and fibroblasts were mainly present in granulomatous dermis (cluster 0), whereas the non-lesional subsets were present in unaffected dermis (cluster 1) (Figures 2E and 2F). We confirmed this observation by projecting the gene expression profiles of lesional and non-lesional macrophages, helper T cells, and fibroblasts onto the spatial transcriptomics profiles across all samples. We observed high activity of lesional gene sets inside granulomas, while non-lesional gene sets were primarily expressed in the surrounding dermis (Figures 2G and S2D).

We further compared our data for skin granulomas with published bulk RNA-seq data for granulomas in lung,[33] orbital adipose tissue, lacrimal gland tissue,[34] and progressive fibrotic lung granuloma tissue.[35] Gene signatures of these granulomas were consistently enriched in lesional skin compared with non-lesional skin, indicating that certain regulatory pathways of granuloma formation are shared across organs (Figure S2E).

In summary, scRNA-seq and spatial transcriptomics uncovered a gene expression profile reminiscent of granuloma-induced cellular activation, which we observed in lesional macrophages, helper T cells, and fibroblasts. The following sections focus more deeply on macrophages (Figure 3), T cells (Figure 4), and structural cells (Figure 5), characterizing each cell type's contribution to granuloma formation and maintenance.

GA macrophages display a strong proinflammatory signature

Skin macrophages are mainly located in the dermal compartment of the skin. Their biological roles include the removal of pathogens and of debris from infected and dead cells.[36] Moreover, macrophages constitute the dominant immune-modulatory cell type in granulomas and are regarded as a major driver of granuloma formation.[2] They contribute to the tightly packed structure of granulomas and promote adaptive immune response and tissue fibrosis.[2,18]

Investigating the role of macrophages in skin granulomas, we performed dimensionality reduction and unsupervised clustering of the single-cell transcriptome profiles of all macrophages. This analysis resulted in two main subclusters. The cells in cluster 0 were associated with lesional skin, whereas the cells in cluster 1 were predominantly derived from non-lesional skin (Figures 3A and S3A). Automated cell-type assignment identified various types of myeloid cells in cluster 1. By contrast, cluster 0 comprised only two macrophage subsets (Figure S3B). Differential gene expression analysis revealed transcriptional profiles that are indicative of chronic activation of the myeloid cells in cluster 0. For example, we found higher mRNA expression of *CD14*, *FCGR3A* (coding for CD16), and *APOC1* but reduced levels of genes related to interleukin-1 (*IL1A*, *IL1B*, *IL1R1*, and *IL1R2*).[37] Based on these results, we refer to the myeloid cells associated with cluster 0 as "granuloma-associated (GA) macrophages" and to the cells of cluster 1 as "homeostatic macrophages" (Figures 3A, 3B, and S3A; Table S3).

GA macrophages showed high mRNA expression of *ACE*, *CHI3L1*, *CHIT1*, *CYP27A1*, and *CYP27B1* (Figure 3B), consistent with bulk gene expression data of cutaneous sarcoidosis.[38,39] *ACE* (coding for angiotensin-converting enzyme) is used in clinical practice as a serum marker for sarcoidosis activity.[40] GA macrophages also expressed elevated levels of *S100A8* and *S100A9* (Figures 3B and S3C); these two genes jointly code for calprotectin, which is secreted by macrophages and neutrophils

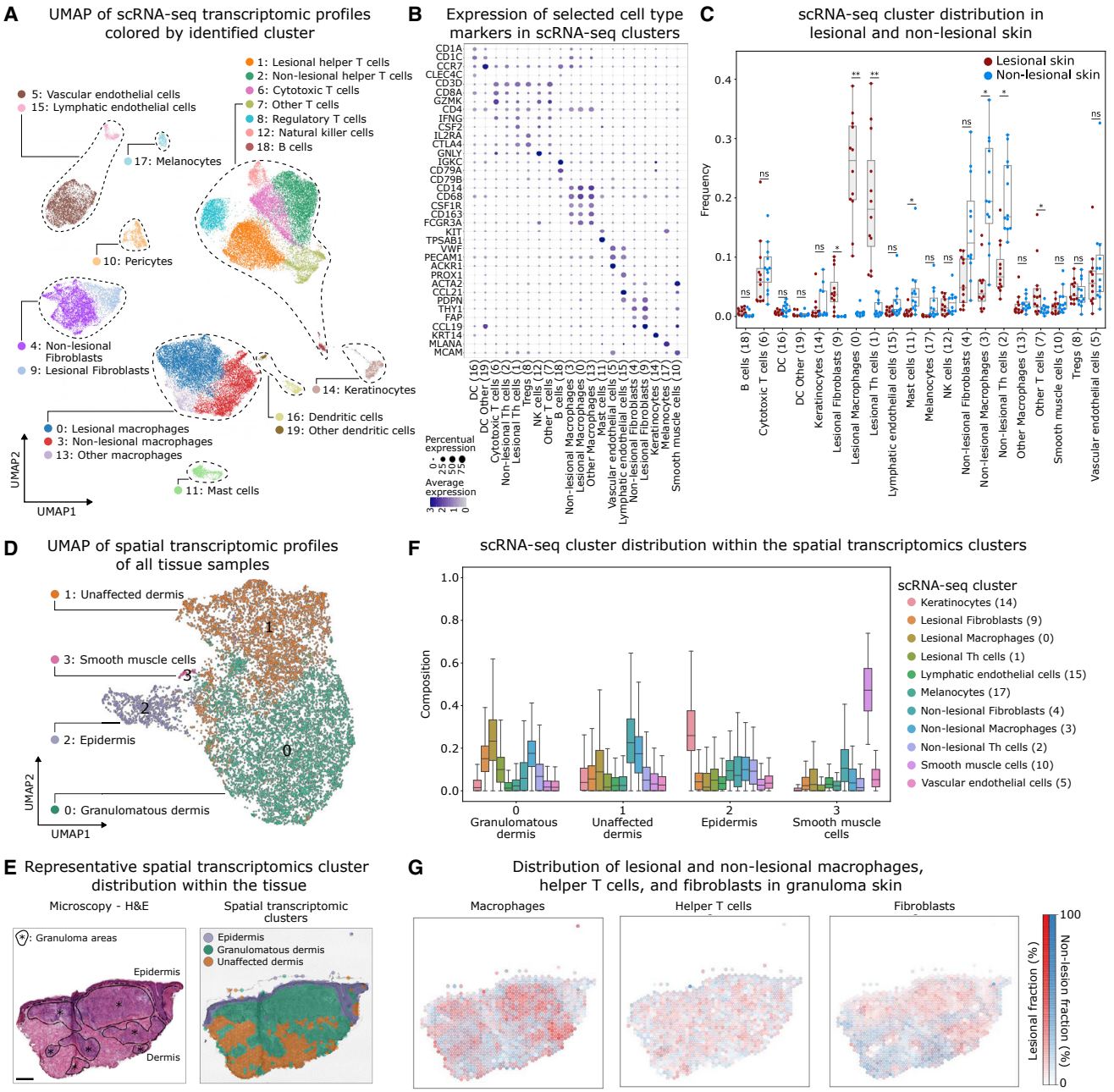

Figure 2. Specific macrophage, T cell, and fibroblast cell subsets accumulate in granulomas

(A) UMAP of scRNA-seq transcriptome profiles, with color-coded cell clustering annotated based on marker gene expression.

(B) Dot plot showing expression of selected marker genes for the cell subsets from (A).

(C) Boxplot displaying the frequency of the cell subsets in lesional and non-lesional skin, based on the scRNA-seq data. *$p < 0.05$, **$p < 0.01$.

(D) UMAP of spatial transcriptome profiles from lesional skin, with color-coded clustering of assay spots in the spatial transcriptomics data. Spot clusters were annotated based on histological assessment.

(E) Spatial transcriptomics data of one representative patient annotated with granuloma-associated spot clusters. Left: H&E staining of lesional skin (from Figure 1D). Scale bar: 500 μm. Right: localization of spot clusters (from D) in the same sample.

(F) Boxplots showing the cellular composition of the spot clusters from (D), based on the scRNA-seq-derived cell subsets (from A).

(G) Localization of scRNA-seq-derived cell signatures from (A) for macrophages (cluster 0 [red] and 3 [blue]), helper T cells (cluster 1 [red] and 2 [blue]), and fibroblasts (cluster 9 [red] and 4 [blue]) for the sample shown in (E). Data in (A)–(D) and (F) are from 12 independent patients.

See also Figure S2 and Table S2.

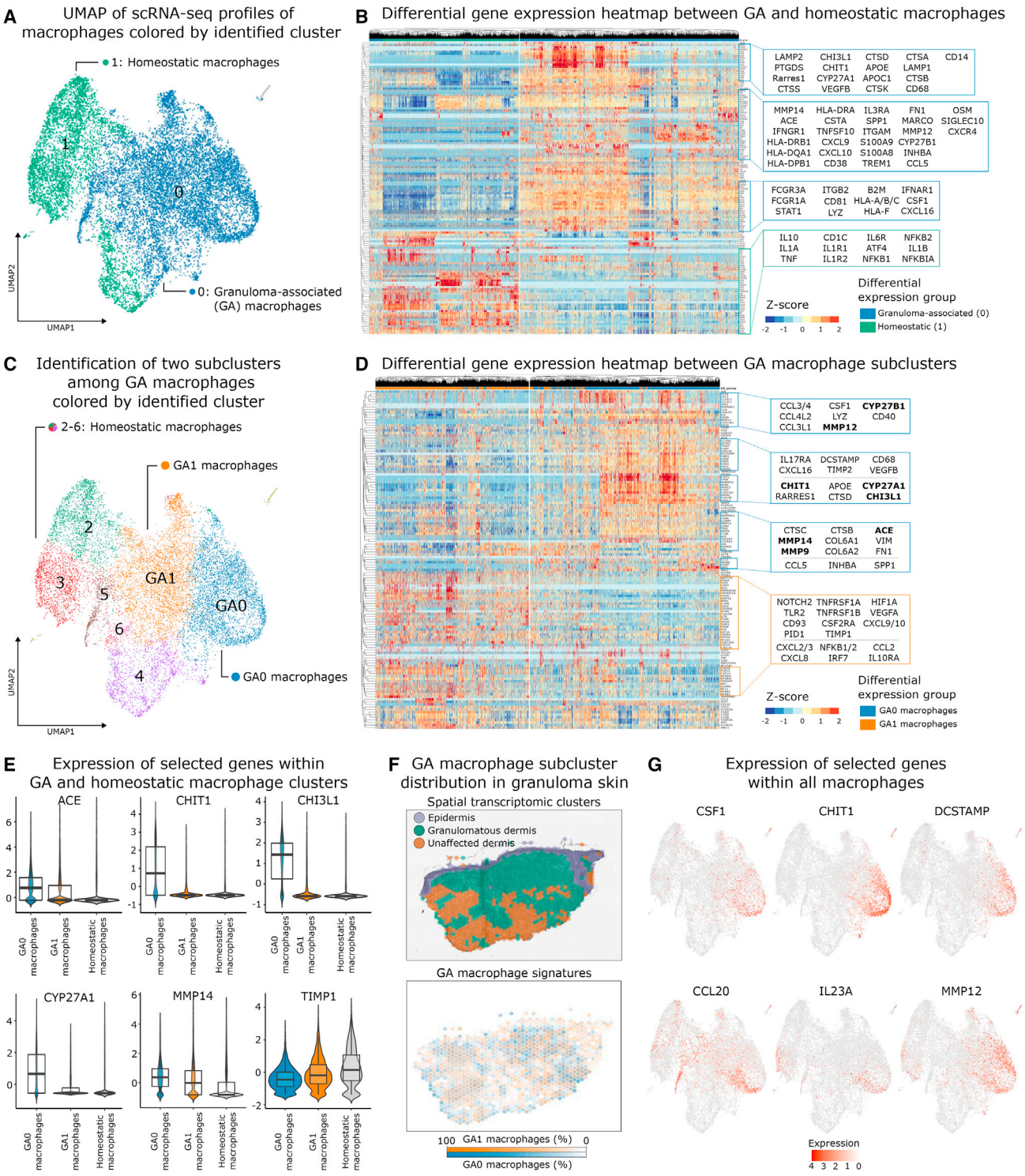

Figure 3. Granuloma-associated macrophages display a strong proinflammatory signature

(A) UMAP of scRNA-seq transcriptome profiles of macrophages from lesional and non-lesional skin, with color-coded cell clustering annotated based on preferential association with lesional (cluster 0) or non-lesional skin (cluster 1).

(B) Clustered scRNA-seq heatmap for differentially expressed genes between granuloma-associated (GA) macrophages (cluster 0) and homeostatic macrophages (cluster 1).

(C) UMAP of scRNA-seq transcriptome profiles as in (A) but clustered with higher granularity (clustering resolution: 0.5 instead of 0.15).

(D) Clustered scRNA-seq heatmap for differentially expressed genes between GA0 macrophages and GA1 macrophages (from C).

(E) Violin plot showing the expression of selected genes in GA macrophages and homeostatic macrophages.

(legend continued on next page)

during inflammation.[41] Moreover, GA macrophages highly expressed *IFNGR1* and showed an upregulation of genes associated with IFN-γ-activated macrophages[42] (*CCL5*, *CXCL9*, *CXCL10*, *CSF2RB*, *FCGR1A*, *HLA-A*, *HLA-B*, *HLA-DQA1*, *IFI27*, *IRF1*, *IRF8*, and *STAT1*), with cell lysis and the lysosome (genes coding for cathepsins, *LAMP2*, and *LYZ*), and with ECM components (*FN1*, *OSM*, and *SPP1*) (Figures 3B and S3C).

Among the upregulated genes, we observed an enrichment for gene sets associated with energy generation and metabolism, antigen processing and presentation, organization of the ECM, mTORC1 signaling, and IFN-γ signaling. By contrast, downregulated genes showed an enrichment for signaling via IL-1, IL-10, TNF-α, and NF-κB, and for apoptosis-related pathways (Figure S3D; Table S4). In support of this non-conventional inflammatory macrophage phenotype, we found inflammation-associated transcription factors upregulated in GA macrophages and expressed inside granulomas (Figures S3E and S3F); this included *RFX5*, *TCF7L2* (coding for TCF4), and *STAT* family members. Our observations in human patient samples are consistent with a mouse model of granuloma formation that identified the checkpoint kinase mTORC1 in macrophages as an inhibitor of NF-κB signaling and apoptosis, leading to persistent granuloma formation.[12] Indeed, we observed increased activity of the mTORC1-dependent transcription factors *SREBF1* and *SREBF2* in GA macrophages (Figures S3E and S3F).

The metabolic signature of GA macrophages also resembles conditions associated with tumor microenvironments, where hypoxic conditions and extracellular acidity contribute to cancer progression.[43–45] *HIF1A* as well as hypoxia-related genes were upregulated in GA macrophages (Figures 3B and S3G; Table S3), and we detected a previously published hypoxia gene signature in areas of granulomatous dermis (Figure S3H).[46] GA macrophages appeared to rely on oxidative phosphorylation and glycolysis to produce energy, and upregulation of pathways involved in pyruvate and lactate production likely contribute to the creation of an acidic milieu in granulomas (Figure S3D; Table S4).

To further characterize the GA macrophages, we re-clustered all macrophages and identified two lesional subclusters: GA macrophage cluster GA0 and GA1 (Figure 3C). We detected higher expression of several sarcoidosis-related genes (*ACE*, *CHI3L1*, *CHIT1*, *CYP27A1*, and *CYP27B1*) in cluster GA0 (Figures 3D and 3E), and we localized the GA0 macrophage gene signature exclusively to sarcoidosis granuloma (Figure 3F). Immunofluorescence protein staining confirmed granuloma-specific expression of chitinase 1 by GA0 macrophages (Figure S3I). Furthermore, we found increased expression of metalloproteinases (*MMP9*, *MMP12*, and *MMP14*) in cluster GA0; these genes play a role in the degradation of the ECM.[47,48] Conversely, the same genes appear to be downregulated in cluster GA1 (Figures 3D and 3E). These results suggest functional heterogeneity between GA1 and GA0 macrophages regarding their ability to regulate immune cell trafficking and maintenance within granulomas.

GA0 macrophages also expressed the *CSF1* gene (Figure 3G), which encodes the macrophage colony stimulating factor (M-CSF), an essential factor for macrophage survival, differentiation, and proliferation. While M-CSF is normally produced by structural cells (e.g., fibroblasts, endothelial cells, and smooth muscle cells), macrophages can also secrete M-CSF and thereby increase local tissue inflammation. High levels of *CSF1* further correlated with elevated expression of the chitin regulator *CHIT1*, the Th17 differentiation-inducing genes *CCL20* and *IL23A*, the matrix metalloproteinase gene *MMP12*, and the cell surface receptor gene *DCSTAMP* (Figure 3G). MMP12 is known to cleave and degrade ECM components including type 1 and type 4 collagens, laminins, entactin, and fibronectin,[49] thus facilitating cell migration through structures such as the basal laminae. DCSTAMP is essential for cell-cell fusion of non-osteoclast multinucleated giant cells,[50,51] suggesting that these inflammatory macrophages of the GA0 subcluster are molecularly equipped to form multinucleated giant cells.

Our data revealed a highly inflammatory environment inside the granulomas that is shaped by GA macrophages. These macrophages support adaptive immune responses and ECM remodeling, thereby contributing to a microenvironment of persistent inflammation in granulomas.

T cells with a Th17.1 phenotype are enriched in granulomas

Tissue-resident $CD3^+$ T cells constitute the main cell type of adaptive immunity in the skin. Under homeostatic conditions, most of them are $CD4^+$ helper T cells located in perivascular areas of the dermis.[52,53] These cells have protective functions during infection, but they can also have pathological effects.[2] In granuloma formation, $CD4^+$ helper T cells amplify local innate immune response by recruiting effector cells to the site of inflammation and supporting their activity.[54] Immunofluorescence protein staining identified $CD3^+$ T cells both inside granulomas and in their immediate vicinity (Figure S4A).

Our scRNA-seq data identified seven clusters of lymphocytes, including helper T cells (clusters 0, 1, and 6), regulatory T cells (cluster 2), cytotoxic CD8 T cells (cluster 3), and NK cells (cluster 5). T cells of cluster 4 displayed a mixed phenotype with both helper T cell and cytotoxic T cell characteristics (*CD3*, *CD4*, *CD8*, and *GZMK*); we refer to them as "other T cells" (Figures 4A and S4B). Helper T cells of cluster 0 comprised lesional and non-lesional skin cells, whereas cells of cluster 1 were predominantly derived from lesional skin (Figure 4A). We thus refer to cluster 0 as homeostatic helper T cells and to cluster 1 as GA helper T cells. These observations suggest that granulomas contain a variety of T cell subsets, with GA helper T cells constituting a granuloma-specific cell subset.

We compared the transcriptional profiles of GA helper T cells with those of homeostatic T cells. Higher expression in GA helper T cells was observed for genes encoding transcription factors (*RORC*, *STAT1*, *STAT5A*, and *TBX21*), cytokines and cytokine receptors (*CSF2*, *IFNG*, and *IL23R*), and chemokines and

(F) Spatial transcriptomics data of one representative patient annotated with GA macrophage gene signatures. Top: localization of spot clusters (from Figure 2E). Bottom: localization of GA0 (blue) and GA1 (orange) macrophage gene signatures (from C) in the same sample.
(G) UMAP (from A) annotated with the expression of selected genes. Data in (A)–(E) and (G) are from 12 independent patients.
See also Figure S3 and Tables S3 and S4.

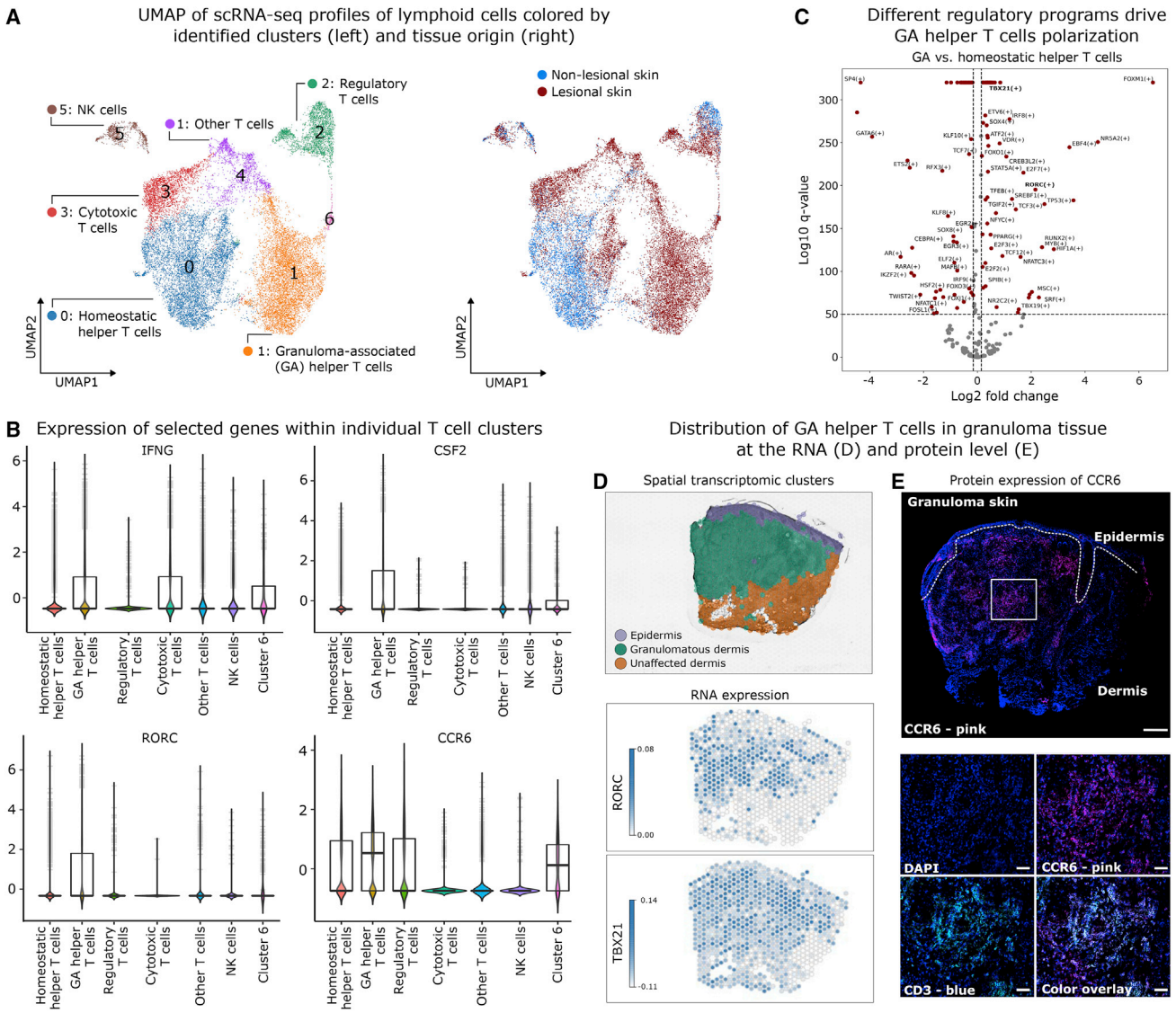

Figure 4. T cells with a Th17.1 phenotype are enriched in granulomas

(A) UMAP of scRNA-seq transcriptome profiles of lymphoid cells from lesional and non-lesional skin. Left: color-coded and annotated based on marker genes and preferential association with lesional (cluster 1) or non-lesional skin (cluster 0). Right: color-coded by sample origin.

(B) Violin plot showing the expression of selected genes in different lymphoid cell subsets.

(C) Volcano plot showing differential gene expression for transcription factors in GA helper T cells, compared with homeostatic helper T cells.

(D) Spatial transcriptomics data of one representative patient analyzed for granuloma-specific gene regulation in T cells. Top: localization of spot clusters (as in Figure 2E). Bottom: expression of the transcription factor genes *RORC* and *TBX21* (encoding T-bet) in the same sample.

(E) Immunofluorescence protein staining of skin granulomas for CCR6 (pink; PE), CD3 (light blue; AF750), and DAPI (dark blue). Scale bars: 500 μm (main panel) and 50 μm (zoom-in panels). Data in (A)–(D) are from 12 independent patients.

See also Figure S4 and Tables S3 and S4.

chemokine receptors (*CCL20*, *CCR6*, and *CXCR3*) (Figures S4C and S4D; Table S3). The lymphotoxin beta gene (*LTB*) was also more highly expressed, consistent with previous *in vivo* studies that linked ectopic expression of lymphotoxins to lymphoid-like structures in inflamed tissue.[55,56] GA helper T cells in cluster 1 showed higher mRNA expression of the immune regulatory genes *PDCD1* (encoding PD-1) and *CTLA4*, indicative of chronic T cell stimulation and consequent T cell exhaustion. Moreover, we observed increased expression of genes involved in cell lysis (*CTSH*, *GZMA*, and *GZMH*), suggesting that these GA helper T cells may have cytotoxic properties (Figure S4C). Gene set enrichment analysis, comparing cluster 0 with cluster 1, identified upregulation of pathways associated with IFN-γ signaling, glycolysis, TCR signaling, leukocyte migration, and Notch signaling, as well as downregulation of pathways involved in autophagy, corticosteroid response, and cell division (Figure S4E; Table S4).

The GA helper T cells thus appear to have acquired a chronically activated Th17.1 phenotype. Th17.1 cells are characterized

by IL-23 and IL-12 driven conversion from Th17 toward a Th1 phenotype.[57,58] These cells activate neutrophils and other myeloid cells by producing high amounts of IFN-γ (*IFNG*) and GM-CSF (*CSF2*) (Figure 4B). Th17.1 cells depend on the joint activity of transcription factors T-bet (encoded by *TBX21*) and Rorγt (encoded by *RORC*),[57] which were indeed co-expressed in GA helper T cells (Figure 4C) and granulomatous skin (Figure 4D). Th17.1 cells are recruited to the site of inflammation via the CCL20-CCR6 axis, where CCL20 is produced by myeloid cells and its receptor CCR6 is expressed on the T cells (Figure 4B). Immunofluorescence protein staining detected CCR6 expression on $CD3^+$ T cells that were localized inside the granulomas (Figures 4E and S4F).

Our results indicate that persistent stimulation within granulomas leads to the differentiation of helper T cells toward a Th17.1 phenotype that promotes macrophage activation and inflammation. Th17.1 cells were previously observed in bronchoalveolar lavage fluid from patients with lung sarcoidosis,[22,59,60] indicating similar T cell responses in granulomas of other organs. The spatial organization of $CD3^+$ T cells in granulomas and the expression of *LTB* by GA helper T cells suggest parallels with the formation of tertiary lymphoid structure (TLS) generation, despite certain differences such as the lack of B cells and plasma cells in granulomas (Figures 2A–2C). In summary, GA helper T cells appear to induce macrophage activation and perform cytotoxic functions in an MHC class II-restricted fashion (complementary to CD8 cytotoxic T cells[61]), ultimately leading to T cell exhaustion in this inflammatory environment.

Structural cells promote local inflammation and tissue remodeling in granulomas

Structural cells, such as endothelial cells and fibroblasts, provide shape and metabolic support to tissues and organs.[62,63] These cell types are characterized by organ-specific gene expression and contribute broadly to immune regulation and response to pathogens.[64] In granuloma formation, fibroblasts are thought to promote fibrosis in response to inflammatory triggers, while endothelial cells are frequently observed in the periphery of granulomas where they provide lymphatic and blood microvasculature.[65]

Among the endothelial cells, we identified two large (cluster 0 and 1) and three smaller subpopulations (Figure S5A). Endothelial cells were transcriptionally more similar between lesional and non-lesional skin than it was the case for macrophages or T cells (Figure 2A). Nevertheless, cluster 0 was primarily associated with lesional skin (“GA endothelial cells”), whereas cluster 1 was enriched in non-lesional skin (“homeostatic endothelial cells”) (Figure S5B). Differential gene expression analysis revealed subtle differences indicative of GA endothelial cells contributing to ECM remodeling, focal adhesion, and cell migration from the circulation into the granulomas (Figure S5C; Table S3).

Among the fibroblasts, we identified three clusters (Figure 5A). Cluster 0 was predominantly associated with non-lesional skin, cluster 1 was dominated by lesional skin, and cluster 2 contained a mix of cells from both sources (Figure S5D). We thus refer to cluster 0 as “homeostatic fibroblasts” and to cluster 1 as “GA fibroblasts,” while cluster 2 (“other fibroblasts”) was excluded from further analysis. In GA fibroblasts, we observed higher expression of the oncostatin M receptor gene (*OSMR*), which promotes the expression of proinflammatory factors,[66] and of *FAP*, *PDPN*, and *THY1*, which are also expressed in fibroblasts isolated from chronically inflamed tissues[67–69] (Figures 5B and S5E; Table S3). Overall, we observed greater cellular heterogeneity in GA fibroblasts than in homeostatic fibroblasts, in part due to the presence of two distinct subsets among GA fibroblasts (Figures 5B and 5C).

First, “immune-interacting fibroblasts” expressed genes involved in cell recruitment and retention (*CCL19*, *CXCL9*, *CXCL10*, and *VCAM-1*), attraction and activation of macrophages (*CCL5*, *CHI3L1*, and *CHI3L2*), antigen presentation (*HLA-A*, *HLA-B*, *HLA-C*, *HLA-F*, and *CD74*), and TGF-beta signaling (*TGFB1*, *TGFB3*, and *TGFBI*) (Figures 5B and S5E). Consequently, gene set enrichment identified an upregulation of immune functions and cellular communication (Figure S5F; Table S4).

Second, “tissue-remodeling fibroblasts” were characterized by high expression of genes that encode components of the ECM (collagen genes, *FN1*, *LOXL1*, *POSTN*, *SPARC*, and *TNC*) as well as regulators of the ECM (*MMP9* and *TIMP1-3*) and of angiogenesis (*VEGFA* and *VEGFC*) (Figures 5B and S5E). We also detected increased expression of *WNT2* and *RUNX2*, two genes involved in cell migration, tumor invasion, and proliferation[70,71] (Figure 5B). Thus, we observed an enrichment for the biological process of collagen and proteoglycan formation, ECM formation, and lymph angiogenesis (Figure S5F).

In lesional skin, GA fibroblasts located adjacent to granulomas showed high mRNA expression of the proinflammatory marker FAP (Figures 5D and S5G). Homeostatic fibroblasts were detected outside granulomas, whereas gene signatures of immune-interacting fibroblasts were detected in close proximity of these structures, and tissue-remodeling fibroblasts were predominantly located inside granulomas, suggesting that ECM constituents are secreted within these inflamed structures (Figure 5D). The importance of ECM remodeling in granulomas was further supported by high expression of collagen IV, both in tissue-remodeling fibroblasts (Figures 5D and S5H) and in granuloma-surrounding endothelial cells (Figures S5C and S5H), and by macrophage-specific mRNA expression of metalloproteinases (*MMP9* and *MMP12*) that are known to degrade ECM proteins including collagen IV (Figures 5B and S5E). A dynamic equilibrium of matrix deposition and degradation may facilitate lymphocyte trafficking while enhancing immune cell adhesion and retention within granulomas.

To identify transcriptional regulators in fibroblasts that contribute to granuloma formation, we compared GA fibroblasts with homeostatic fibroblasts (Figure 5E). GA fibroblasts were characterized by the expression of immune-associated transcription factors including *IRF8*, *RELB*, and *STAT2*. We also detected higher expression of *SPI1* (coding for PU.1), which controls fibroblast polarization and pro-fibrotic functions.[72] Together with BATF3 and IRF8 (both more active in GA fibroblasts), PU.1 promotes re-programming of fibroblasts into antigen-presenting cells.[73] Moreover, analysis of the two GA fibroblast subsets identified higher mRNA levels of transcription factors associated with development (*HOXC6*, *HOXC9*, *NR2F2*, and *TBX15*) and IFN response (*IRF3*, *IRF5*, *IRF8*, *IRF9*, and *STAT2*) in immune-interacting compared with tissue-remodeling

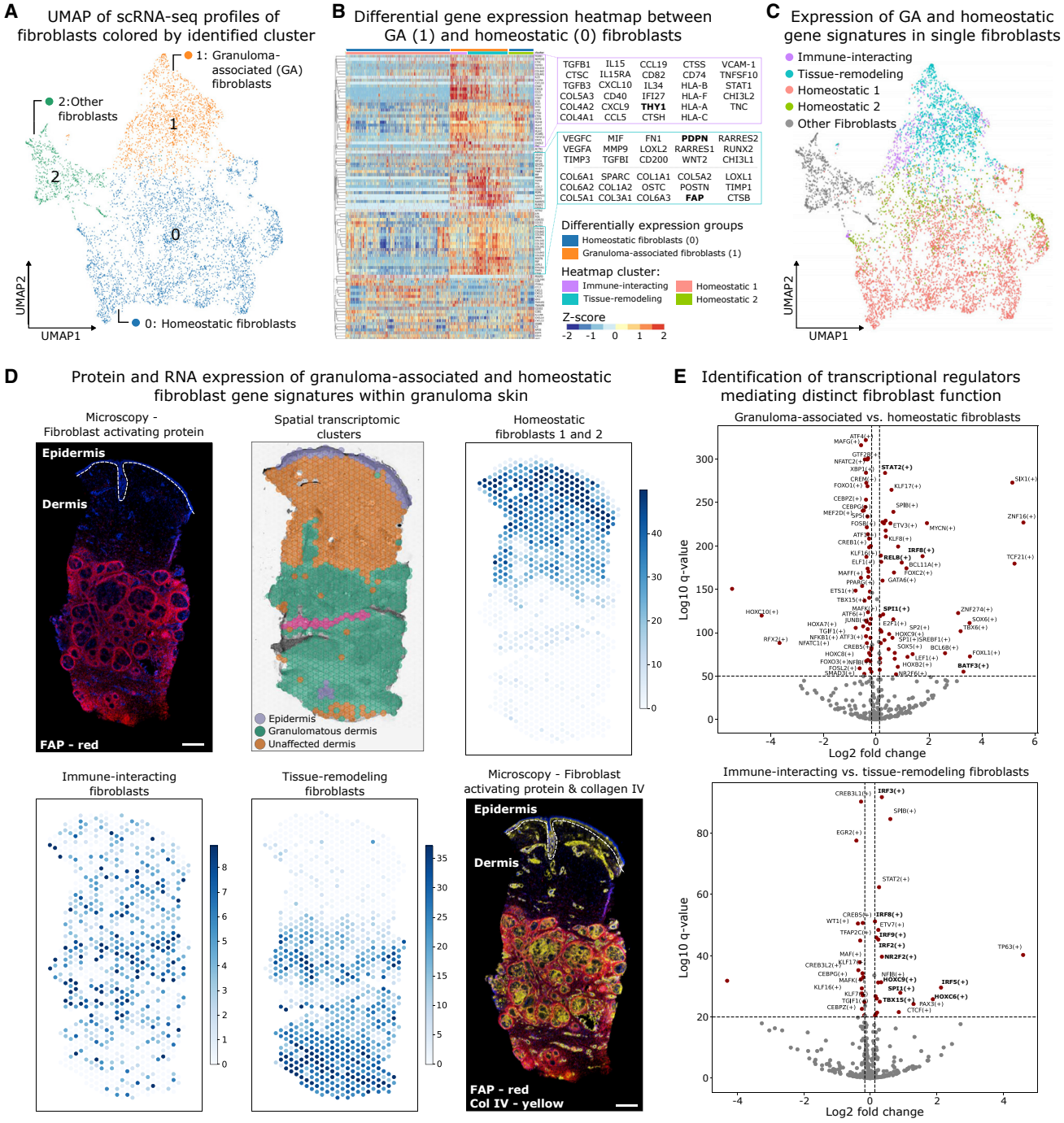

Figure 5. Structural cells promote local inflammation and tissue remodeling in granulomas

(A) UMAP of scRNA-seq transcriptome profiles of fibroblasts from lesional and non-lesional skin, with color-coded cell clustering annotated based on preferential association with lesional (cluster 1) or non-lesional skin (cluster 0).

(B) Clustered scRNA-seq heatmap for differentially expressed genes between granuloma-associated (GA) fibroblasts and homeostatic fibroblasts.

(C) UMAP of scRNA-seq transcriptome profiles as in (A) but color-coded and annotated with differential gene signatures from (B).

(D) Spatial profiling data of one representative patient annotated with fibroblast subsets. Top left: immunofluorescence protein staining of skin granulomas for FAP (red; APC) and DAPI (dark blue); the basal membrane between dermis and epidermis is indicated with a dotted line. Top center: localization of spot clusters (as in Figure 2E). Top right, bottom left, and bottom center: localization of gene signatures (from C) in the spatial transcriptomics data for the same sample. Bottom right: immunofluorescence protein staining of the same sample for FAP (red; APC), collagen IV (yellow; PE), and DAPI (dark blue). Scale bars: 500 μm.

(E) Volcano plot showing differential gene expression of transcription factors in fibroblast subsets. Top: comparison of GA fibroblasts and homeostatic fibroblasts (from A). Bottom: comparison of immune-interacting fibroblasts and tissue-remodeling fibroblasts (from D). Data in (A)–(C) and (E) are from 12 independent patients. See also Figure S5 and Tables S3 and S4.

fibroblasts. *IRF5* in particular is known to promote inflammatory macrophage polarization.[74] Differential expression of these transcription factors is likely to contribute to the observed innate-like functions and the inflammatory phenotype in skin granulomas.

Our results highlight fibroblasts and their role in ECM remodeling as promising therapeutic targets in granulomatous diseases. We identified two types of GA fibroblasts: immune-interacting fibroblasts that are involved in the attraction, activation, and retention of immune cells; and tissue-remodeling fibroblasts that contribute to the shape and structure of granulomas. Moreover, for endothelial cells we uncovered a characteristic spatial distribution inside granulomas. This is reminiscent of the formation of ''high endothelial venules'' that facilitate lymphocyte entry into lymphoid structures.[75] Together, these results underline the contribution of structural cells to granuloma formation and maintenance.

Cellular crosstalk of immune and structural cells defines the granuloma structure

Our single-cell and spatial profiling identified multiple subsets of macrophages (Figure 3), T cells (Figure 4), and fibroblasts (Figure 5) that are localized inside granulomas. To understand the interplay of these cell types in granuloma formation, we used this dataset to predict cell-cell interactions based on ligand-receptor expression[76] and to analyze the cellular crosstalk (Figure S6A; Table S5).

GA macrophages, T cells, and fibroblasts expressed numerous chemokines and chemokine receptors that predict cell-cell interactions (e.g., *CXCR3* with *CXCL9*, *CXCL10*, *CXCL11*, and *CCL19*; *CCR5* and *CCR1* with *CCL5*; and *CCR7* with *CCL19*). We also confirmed several inflammation-linked interactions discussed in previous sections (*CCR6* with *CCL20*; *GMCSFR* with *CSF2*; and *CSF1R* with *CSF1*), which were significantly enriched (Figure 6A; Table S5) and observed inside granulomas, based on the spatial transcriptomics data (Figures 6A, 6B, 6D, and S6B).

Many interactions were cell-type specific. GA helper T cells expressed *IFNG* that acts on *IFNGR1*-expressing cells such as macrophages and structural cells (Figure 6A; Table S5). GA helper T cells also expressed *LTB*, whereas the corresponding receptor *LTBR* was expressed in macrophages, fibroblasts, and endothelial cells; this interaction was most prevalent inside granulomas (Figures 6A and S6B). In lymphoid organ formation, LTB leads to the secretion of VEGF-C by fibroblasts, promoting endothelial cell development and inducing expression of adhesion molecules on endothelial cells.[77] Indeed, we detected LTB pathway activity in GA fibroblasts, where it appears to induce vascular endothelial growth factors (*VEGFA* and *VEGFC*) and various collagens, which can promote angiogenesis and vascular supply by acting on VEGFR1 (*FLT1*), VEGFR2 (*KDR*), and integrins in endothelial cells (Figure S6B). Furthermore, we detected *PECAM1* (coding for CD31) expression in endothelial cells, which predicts interactions with *CD38*-expressing GA macrophages and GA helper T cells within granulomas (Figure 6B), and this interplay was confirmed by immunofluorescence protein staining (Figure 6C).

Beyond cellular crosstalk mediated by secreted factors, we also identified gene pairs that control structural interactions and adhesional support to neighboring cells.[64] Various integrins were expressed in fibroblasts (*CD44* and *ITGA9*), T cells (*ITGA4*, coding for integrin a4, also called CD49d), and endothelial cells (*ITGAV*, *ITGA5*, and *ITGA9*), which mediate binding to ECM components (*FN1*, *SPP1*, and *TNC*) and collagens (Figures 6D and S6B; Table S5). For example, the integrin aV (*ITGAV*), which is expressed by endothelial cells and macrophages (Table S5), promotes interstitial migration along fibronectin fibers.[78] By contrast, *ITGA4* is highly expressed in GA helper T cells; it codes for a protein that mediates exfiltration of leukocytes from the vasculature into tissue and binds *TNC*, VCAM-1, and osteopontin (*SPP1*).[79] Osteopontin signaling also promotes differentiation of Th1 and Th17 cells and prolongs their survival.[80] These interactions are supported by expression of *SPP1-CD44* and *FN1-a4b1* inside granulomas (Figures 6A and 6D), which we validated by immunofluorescence protein staining (Figure 6E). These results suggest that aberrant production of ECM components by fibroblasts and macrophages leads to ECM remodeling, which is expected to contribute to the proinflammatory environment of granulomas and may create tracks for cell migration that guide immune cells inside the granulomas.

We also observed significant enrichment of several immune regulatory mechanisms. First, we detected high expression of *DPP4* in GA fibroblasts and GA helper T cells (Figure 6A). This gene encodes CD26, a cell surface enzyme that induces post-translational modification of chemokines, such as CXCL9 and CXCL10, and alters leukocyte trafficking.[81] Indeed, we observed frequent co-localization of *DPP4* and *CXCL10* expression inside granulomas (Figure S6B). Second, the immune regulatory gene *CTLA4* was highly expressed in T cells, and its interaction partners *CD80* and *CD86* were expressed on GA macrophages within granuloma structures (Figures 6A and S6B). Third, high expression of *PDCD1* (which encodes the immune checkpoint receptor PD-1) and *CD274* (which encodes the corresponding ligand PD-L1) was observed inside granulomas (Figure 6A), and the co-localization of the corresponding proteins was confirmed by immunofluorescence protein staining (Figure S6C). PD1-expressing T cells and PD-L1-expressing macrophages were increased in granulomas, compared with non-inflamed skin (Figure S6D), which may over time contribute to the exhaustion of T cells[82] inside granulomas. Finally, *IL23* and *IL23R* were also highly expressed in granulomas and may help create a cellular environment that favors the Th17.1 cell phenotype (Figures 6A and S6B).

Our data thus predict a dense mesh of cell-cell interactions between macrophages, T cells, and structural cells inside granulomas, which likely contributes to the proinflammatory environment and to the attraction and retention of immune cells that drive sarcoidosis pathology. Aggregating the observations from our study into an overview of the cellular and molecular properties of granulomas (Figure 7A), we highlight three regulatory processes as critical for granuloma formation: (1) angiogenesis and immunometabolism, (2) cytokine and chemokine signaling, and (3) ECM remodeling.

Granulomas share key characteristics with TLSs

Our data uncovered similarities between granulomas (Figure 7A) and TLSs—which are lymphoid aggregates in non-lymphoid tissues that form in the vicinity of tumors or sites of infection and contribute to an effective immune response.[75] We validated the global transcriptional similarity between

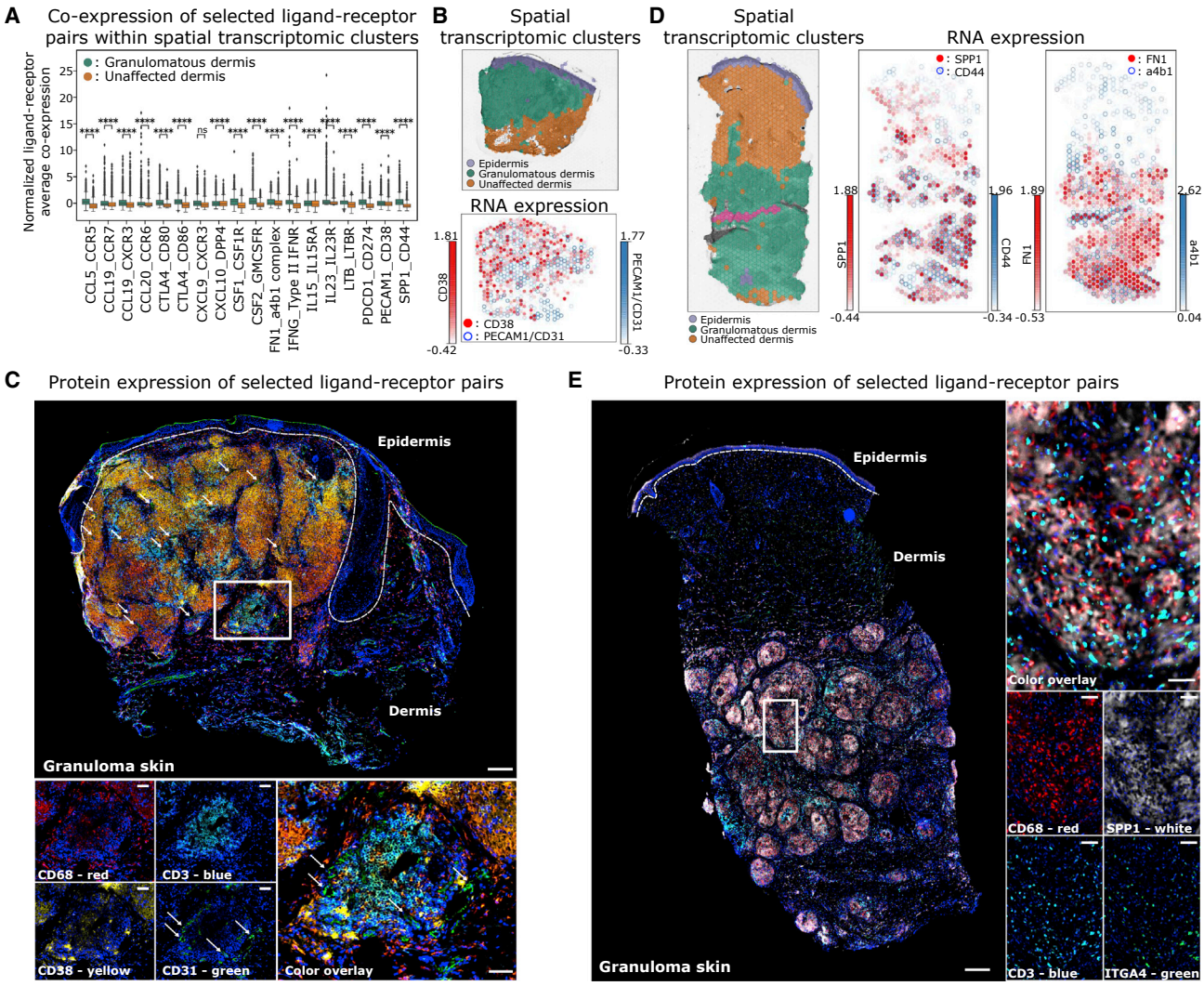

Figure 6. Cellular crosstalk of immune and structural cells defines the granuloma structure

(A) Bar plot showing co-expression for selected ligand-receptor pairs based on the spatial transcriptomics data for granulomatous dermis (green) and unaffected dermis (orange). ****$p < 0.0001$.

(B) Spatial profiling data for one patient analyzed for ligand-receptor-mediated cell-cell interactions. Top: localization of spot clusters (as in Figure 2E). Bottom: gene expression based on the spatial transcriptomics data for the ligand-receptor pair CD38 (red) and CD31 (blue).

(C) Immunofluorescence protein staining of skin granulomas for CD68 (red; APC), CD3 (light blue; AF750), CD38 (yellow; PE), CD31/PECAM1 (green; FITC), and DAPI (dark blue). White arrows indicate endothelial cells. Scale bars: 500 μm (main panel) and 50 μm (zoom-in panels).

(D) Spatial profiling data of a second patient analyzed for ligand-receptor-mediated cell-cell interactions. Left: localization of spot clusters (as in Figure 2E). Center and right: gene expression based on the spatial transcriptomics data for the ligand-receptor pairs SPP1 (red) and CD44 (blue) as well as FN1 (red) and integrin a4b1.

(E) Immunofluorescence protein staining of skin granulomas for CD68 (red; APC), CD3 (light blue; PE-TR), SPP1 (light pink; AF750), ITGA4 (green; FITC), and DAPI (dark blue). Scale bars: 500 μm (main panel) and 50 μm (zoom-in panels). Data in (A) is from 12 independent patients.

See also Figure S6 and Table S5.

granulomas and TLSs by investigating an established TLS signature comprising 12 chemokines[83] and found it highly expressed in granulomas (Figures 7B and 7C). Specifically, *CCL5*, *CXCL9*, and *CXCL10* were upregulated in GA macrophages, *CCL4* and *CCL5* in GA T cells, and *CCL5*, *CCL19*, *CXCL9*, *CXCL10*, as well as *CXCL11* were upregulated in GA fibroblasts (Figure 7D). We also observed granuloma-specific activity of the CCL19-CCR7/CXCR3 pathway, which is involved in T cell homing to lymphoid organs (Figures 7E and S7A). We further validated this observation with two additional TLS signatures[84,85] and again found high similarity between granulomas and TLSs (Figures S7B–S7D).

These results suggest that granulomas employ some of the same biological processes that underlie TLS formation. Yet, we also observe characteristic differences. For example, helper T cells in granulomas foster macrophage activation rather than attenuate inflammation as observed in cancer (Figure S7E). We therefore conclude that granuloma formation constitutes a

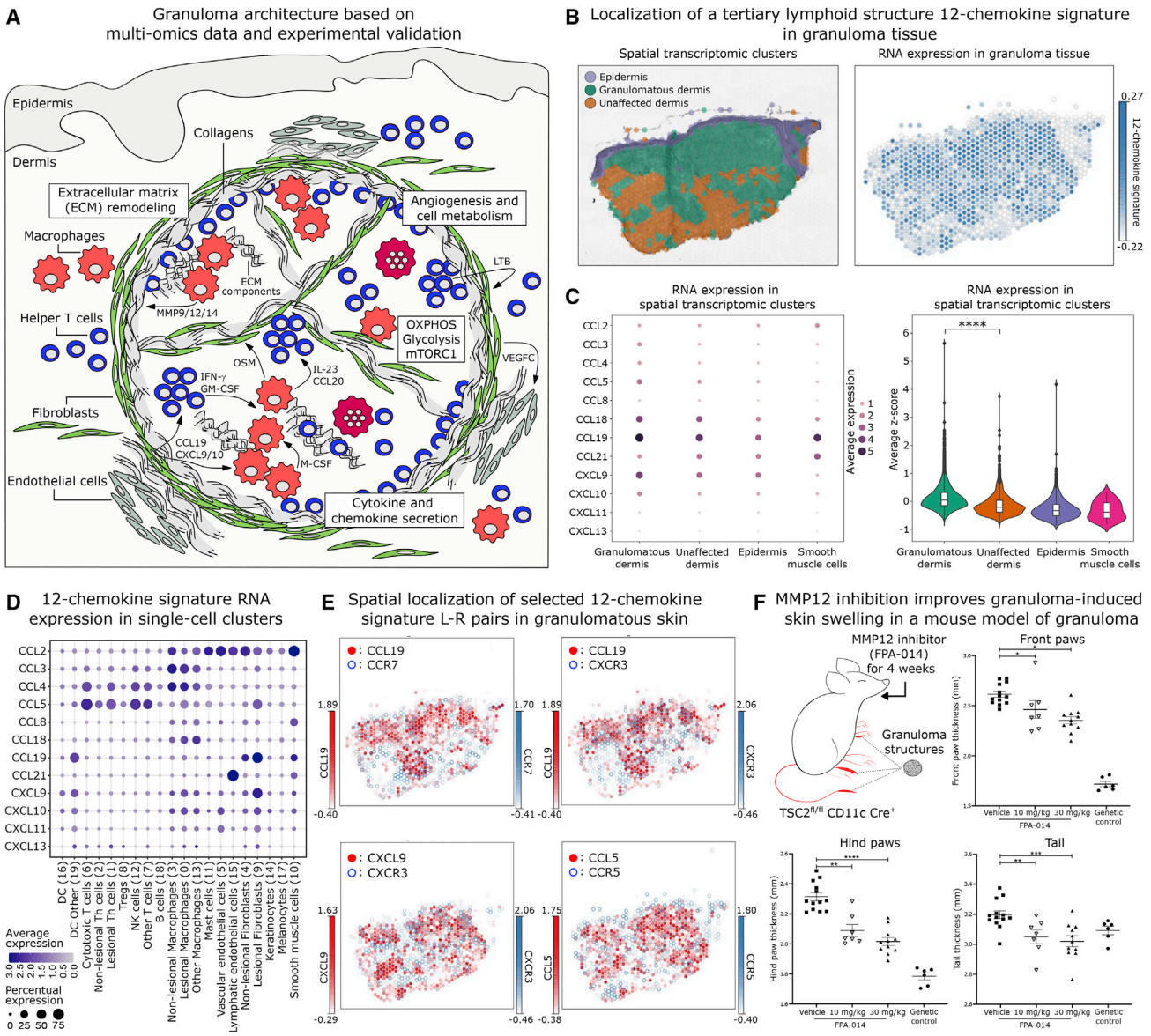

Figure 7. Granulomas share key characteristics with tertiary lymphoid structures

(A) Schematic of the molecular and cellular architecture of granulomas, based on single-cell and spatial profiling of lesional and non-lesional skin from 12 patients with sarcoidosis.

(B) Spatial transcriptomics data of one representative patient analyzed for characteristics of lymphoid organs. Left: localization of spot clusters (as in Figure 2E). Right: expression of a published 12-chemokine gene signature associated with tertiary lymphoid structures (TLSs).[83]

(C) Expression of the same gene signature as in (B) for the spatial transcriptomics spot clusters. Left: dot plot showing the expression of the signature's individual genes for each of the spot clusters (from Figure 2D). Right: violin plot showing the expression distribution of the gene signature across spot clusters.

(D) Dot plot showing the expression of the signature's individual genes for each of the scRNA-seq cell clusters (from Figure 2A).

(E) Gene expression based on the spatial transcriptomics data (same patient as in B) for the signature genes that encode ligands (red: CCL19, CXCL9, and CCL5) and receptors (blue: CCR3, CCR7, and CCR5).

(F) Therapeutic targeting of extracellular matrix remodeling in a mouse granuloma model. Top left: schematic of the granuloma model. $TSC2^{fl/fl}$ CD11c Cre+ mice received the MMP12 inhibitor FPA-014 by oral gavage (n = 7 with 10 mg/kg; n = 11 with 30 mg/kg; n=13 with vehicle control). $TSC2^{fl/fl}$ CD11c Cre− mice (n = 6) were used as genetic controls. Right and bottom: lesion severity assessed by the thickness of the front paw, hind paw, and tail. For each mouse, the average of five individual measurements was taken. The plots show mean values across all treated mice, with error bars representing the standard error of the mean of five independent experiments. *p < 0.05, **p < 0.01, ***p < 0.001, ****p < 0.0001. Data in (C) and (D) are from 12 independent patients.

See also Figure S7 and Table S6.

deregulated and aberrant form of lymphoid organ, utilizing similar regulatory mechanisms but failing to recapitulate the tight control of physiologically normal TLSs.

To generalize our observations beyond the skin, we compared bulk RNA-seq data of granulomas in lung,[33] orbital adipose tissue, lacrimal gland tissue,[34] and progressive fibrotic lung granuloma tissue[35] with our scRNA-seq analysis of skin granulomas. We observed shared expression of regulator genes expressed across multiple cell types, such as *CXCR4*, *HLA-DRB1*, *HLA-DQA1*, *JUNB*, *LYZ*, *PARP14*, *SOCS3*, *SOD2*, and *TYMP*. Certain cell-type-specific genes were also shared by granulomas in other tissue, including genes involved in Th17.1 signaling (*CSF2*, *CSF2R*, and *STAT1*), macrophage activation (*CHIT1*, *LYZ*, and *CSF1R*), TLS formation (*CCL5*, CCL18, and CXCL9), and ECM remodeling (*ADAMDEC1*, *MMP9*, *MMP12*, *CHI3L1*, *SPP1*, and *POSTN*) (Figure S7F). To assess whether these processes were specific to GA inflammation or broadly shared with other inflammatory conditions, we compared our gene expression data with gene signatures of idiopathic pulmonary fibrosis and non-specific interstitial pneumonia (NSIP). We did not observe strong overlaps, indicating that the observed regulatory mechanisms are indeed specific to GA inflammation (Figure S7G).

Exploring the translational and future therapeutic potential of our observations, we pharmacologically targeted the matrix metalloproteinase MMP12 with the investigational drug FPA-014, using a mouse model of granuloma formation (Figure 7F).[12] The *MMP12* gene, which codes for macrophage elastase, was expressed in granulomas from several organs (Figure S7F) and strongly upregulated in GA macrophages in our dataset (Figures 3D and 3G). MMP12 may play a role in GA ECM formation and immune cell activation, and its expression has been shown to correlate with clinical progression in lung granulomas.[33,47] Treating mice with the MMP12 inhibitor FPA-014 over a 4-week period resulted in significantly reduced granuloma-induced skin swelling of the extremities and the tail, compared with control treatment (Figure 7F). These results support a functional contribution of matrix metalloproteinases in granuloma formation and maintenance, likely mediated by their role as ECM modulators and immune cell activators.

In summary, our study mapped the granuloma-specific profiles of innate, adaptive, and structural cells with single-cell and spatial resolution. We identified macrophages with an activated phenotype and altered cell metabolism at the core of the granulomas, shaping an inflammatory microenvironment and attracting other immune cells and structural cells. GA helper T cells with a Th17.1 phenotype were found to interact with and enhance macrophage activation by secreting IFN-γ and GM-CSF. Fibroblasts appear to shape the structure of granulomas by regulating the ECM together with macrophages. These three cell types account for the vast majority of cells in granulomas and are predicted to maintain close cellular crosstalk. They collectively create an aberrant form of TLSs that is fueled by persistent inflammation and immune cell activation (Figure 7A).

DISCUSSION

Granulomas have an important role in pathogen control, but their inappropriate formation and maintenance can give rise to chronic diseases such as sarcoidosis. Here, we charted the cellular and molecular landscape of granulomas of the skin, combining scRNA-seq, spatial transcriptomics, immunofluorescence protein staining, and integrative bioinformatics for 12 well-characterized patients with sarcoidosis. We characterized the major GA cell types and subsets, and we mapped the spatial and regulatory landscape of cell-cell interactions between macrophage, T cells, and fibroblasts.

GA macrophages were characterized by metabolic reprogramming toward increased glycolysis and oxidative phosphorylation—metabolic pathways involved in acute inflammation as well as tissue regeneration and remodeling.[86] We additionally observed upregulation of mTOR signaling, consistent with a recent mouse model of sarcoidosis that is based on induced mTOR activity.[12] Both in our human data and in the mouse model, macrophages downregulated apoptosis signaling, which may contribute to granuloma persistence and chronic inflammation. Moreover, macrophages and fibroblasts jointly contribute to a granuloma-specific microenvironment resembling that of solid tumors, with hypoxia-related gene pathways indicating an acidic environment and enhanced metabolism.[87]

T cells constitute the second major cell type in granulomas. We found high expression of integrins regulating activation and cell migration of T cells inside granulomas, and we detected cytotoxic properties of helper T cells. Furthermore, we observed helper T cells with a Th17.1 phenotype, consistent with previous observations.[22,59] These Th17.1 cells produce high amounts of IFN-γ, GM-CSF, and LTB, which contribute to the continued activation of immune and structural cells inside granulomas.

Fibroblasts are the most prevalent non-hematopoietic cell type in granulomas. We identified two subsets of GA fibroblasts: immune-interacting fibroblasts and tissue-remodeling fibroblasts. The immune-interacting fibroblasts appear to act like a non-hematopoietic immune cell[64,88] and contribute broadly to the activation, attraction, and retention of both immune and structural cells in granulomas. By contrast, the tissue-remodeling fibroblasts promote ECM remodeling, together with GA macrophages, thereby shaping the characteristic granuloma microenvironment.[89]

Collectively, our single-cell and spatial analyses uncovered similarities between granulomas and lymphoid organs (most notably TLSs), both in their spatial organization and the expressed chemokine profile. This similarity is not unexpected given that biological processes underlying granuloma formation, such as infections and chronic inflammation, are also known to trigger the formation of TLSs.[75] While TLSs typically have a defined cause and subside their activity once this cause is resolved,[85] we propose that granulomas constitute a form of aberrant lymphoid organ that uses similar mechanisms as TLSs to form but lacks self-limitation, which makes it prone to become chronic and highly damaging to the host.

While our dataset focuses on granulomas of the skin, we validated and extended our results to granulomas in other organs, based on bulk RNA-seq datasets. Key mediators of granuloma formation were shared across organs, and we selected one such protein—the matrix metalloproteinases MMP12—for functional validation. We found that pharmacological inhibition in a mouse model of sarcoidosis interfered with granuloma formation, consistent with genetic evidence in a separate mouse model.[47] We anticipate that our dataset and methodology can

help identifying promising strategies for interfering with granuloma formation in sarcoidosis and potentially with other granulomas of non-infectious etiology.

In summary, we found that granulomas repurpose transcription regulatory programs of normal lymphoid organ development and are driven by three key processes: changes of immunometabolism, altered cytokine and chemokine pathways, and regulation of integrins and ECM. Our analyses establish an integrated molecular and spatial landscape of non-infectious granulomas and provide a rich dataset for therapeutic targeting of the biological processes underlying granuloma formation.

Limitations of the study

While this study provides a thorough characterization of the *in vivo* architecture of human granulomas, it is subject to certain limitations. First, sarcoidosis is known to show great variability across individuals,[19] which our relatively small patient cohort cannot fully reflect. Second, we focused on granulomas of the skin, with validation against bulk RNA-seq data of granulomas in four other tissues. It will be interesting in the future to dissect the interplay of granulomas across different tissue types in more detail. Third, the role of ECM remodeling in sarcoidosis remains contradictory. Our pharmacological targeting of matrix metalloproteinases provides an initial functional validation of inhibited ECM remodeling as a potential therapeutic approach. In contrast, interfering with ECM components in a murine tuberculosis granuloma model has been shown to aggravate the disease.[90] Clearly, additional work in several preclinical models will be needed to better assess the future potential for treating different granuloma etiologies.

STAR★METHODS

Detailed methods are provided in the online version of this paper and include the following:

- KEY RESOURCES TABLE
- RESOURCE AVAILABILITY
  - Lead contact
  - Materials availability
  - Data and code availability
- METHOD DETAILS
  - Patients and sample collection
  - Flow cytometry and cell sorting
  - Single-cell RNA sequencing
  - Spatial transcriptomics
  - Immunofluorescence protein staining of patient samples
  - Sarcoidosis mouse model and MMP12 treatment
  - Preprocessing and analysis of scRNA-seq data
  - Preprocessing and analysis of spatial transcriptomics data
  - Statistical analysis of immunofluorescent protein staining

SUPPLEMENTAL INFORMATION

Supplemental information can be found online at https://doi.org/10.1016/j.immuni.2023.01.014.

ACKNOWLEDGMENTS

We thank all patients for their participation in the clinical study and for their willingness to donate tissue samples for research. We also thank the Biomedical Sequencing Facility (BSF) at the CeMM Research Center for Molecular Medicine of the Austrian Academy of Sciences for assistance with next-generation sequencing, Foresee Pharmaceuticals for providing the MMP12 inhibitor FPA-014, and all members of the Bock and Stary labs for their help and advice. This work was funded in part by a Vienna Science and Technology Fund project (WWTF LS18-058) (to G.S., T.K., and T.W.). G.S. is supported by a grant from the LEO Foundation (LF-OC-21-000806), an Austrian Central Bank Anniversary Fund project (no. 17872), and an Austrian Science Fund grant (FWF P31494). C.B. is supported by two Austrian Science Fund (FWF) Special Research Program grants (FWF SFB F6102 and FWF SFB F7002) and an ERC Consolidator Grant (grant agreement no. 101001971).

AUTHOR CONTRIBUTIONS

Conceptualization, C.B., G.S., T.K., and T.W.; methodology, C.B., G.S., A.R., and T.K.; investigation, A.K., A.R., C.X.L., C.M., D.A., K.D., L.K., L.U., M.G., P.R., S.S., and T.K.; formal analysis & data curation, D.B., D.R., and L.D.; visualization, A.R., D.B., D.R., L.D., K.D., and T.K.; writing – original draft, A.R. and T.K.; writing – review & editing, A.R., C.B., C.X.L., D.A., D.B., D.R., G.S., K.D., L.D., L.K., L.U., M.G., T.K., and T.W.; supervision, C.B. and G.S.

DECLARATION OF INTERESTS

C.B. is a cofounder and scientific advisor of Myllia Biotechnology and Neurolentech.

INCLUSION AND DIVERSITY

We support inclusive, diverse, and equitable conduct of research.

Received: March 2, 2022
Revised: August 27, 2022
Accepted: January 13, 2023
Published: February 6, 2023

REFERENCES

1. Adams, D.O. (1976). The granulomatous inflammatory response. A review. Am. J. Pathol. *84*, 164–192.
2. Pagán, A.J., and Ramakrishnan, L. (2018). The formation and function of granulomas. Annu. Rev. Immunol. *36*, 639–665. https://doi.org/10.1146/annurev-immunol-032712-100022.
3. Mornex, J.F., Leroux, C., Greenland, T., and Ecochard, D. (1994). From granuloma to fibrosis in interstitial lung diseases: molecular and cellular interactions. Eur. Respir. J. *7*, 779–785. https://doi.org/10.1183/09031936.94.07040779.
4. Roda, G., Chien Ng, S., Kotze, P.G., Argollo, M., Panaccione, R., Spinelli, A., Kaser, A., Peyrin-Biroulet, L., and Danese, S. (2020). Crohn's disease. Nat. Rev. Dis. Primers *6*, 22. https://doi.org/10.1038/s41572-020-0156-2.
5. Saketkoo, L.A., Russell, A.-M., Jensen, K., Mandizha, J., Tavee, J., Newton, J., Rivera, F., Howie, M., Reese, R., Goodman, M., et al. (2021). Health-related quality of life (Hrqol) in sarcoidosis: diagnosis, management, and health outcomes. Diagnostics (Basel) *11*, 1–35. https://doi.org/10.3390/diagnostics11061089.
6. Moradkhani, A., Beckman, L.J., and Tabibian, J.H. (2013). Health-related quality of life in inflammatory bowel disease: psychosocial, clinical, socioeconomic, and demographic predictors. J. Crohns Colitis *7*, 467–473. https://doi.org/10.1016/j.crohns.2012.07.012.
7. Mukhopadhyay, S., Farver, C.F., Vaszar, L.T., Dempsey, O.J., Popper, H.H., Mani, H., Capelozzi, V.L., Fukuoka, J., Kerr, K.M., Zeren, E.H., et al. (2012). Causes of pulmonary granulomas: a retrospective study of 500 cases from seven countries. J. Clin. Pathol. *65*, 51–57. https://doi.org/10.1136/jclinpath-2011-200336.

8. Terziroli Beretta-Piccoli, B., Mainetti, C., Peeters, M.A., and Laffitte, E. (2018). Cutaneous granulomatosis: a comprehensive review. Clin. Rev. Allergy Immunol. *54*, 131–146. https://doi.org/10.1007/s12016-017-8666-8.

9. Adams, D.O. (1974). The structure of mononuclear phagocytes differentiating in vivo. I. Sequential fine and histologic studies of the effect of bacillus Calmette-Guerin (BCG). Am. J. Pathol. *76*, 17–48.

10. Helming, L., and Gordon, S. (2007). The molecular basis of macrophage fusion. Immunobiology *212*, 785–793. https://doi.org/10.1016/j.imbio.2007.09.012.

11. Dawa, S., Menon, D., Arumugam, P., Bhaskar, A.K., Mondal, M., Rao, V., and Gandotra, S. (2021). Inhibition of granuloma triglyceride synthesis imparts control of Mycobacterium tuberculosis through curtailed inflammatory responses. Front. Immunol. *12*, 722735. https://doi.org/10.3389/fimmu.2021.722735.

12. Linke, M., Pham, H.T.T., Katholnig, K., Schnöller, T., Miller, A., Demel, F., Schütz, B., Rosner, M., Kovacic, B., Sukhbaatar, N., et al. (2017). Chronic signaling via the metabolic checkpoint kinase mTORC1 induces macrophage granuloma formation and marks sarcoidosis progression. Nat. Immunol. *18*, 293–302. https://doi.org/10.1038/ni.3655.

13. Wynn, T., and Cheever, A.W. (1995). Cytokine regulation of granuloma formation in schistosomiasis. Curr. Opin. Immunol. *7*, 505–511. https://doi.org/10.1016/0952-7915(95)80095-6.

14. Cadena, A.M., Fortune, S.M., and Flynn, J.L. (2017). Heterogeneity in tuberculosis. Nat. Rev. Immunol. *17*, 691–702. https://doi.org/10.1038/nri.2017.69.

15. Globig, A.M., Hennecke, N., Martin, B., Seidl, M., Ruf, G., Hasselblatt, P., Thimme, R., and Bengsch, B. (2014). Comprehensive intestinal T helper cell profiling reveals specific accumulation of IFN-γ+IL-17+coproducing CD4+ T cells in active inflammatory bowel disease. Inflamm. Bowel Dis. *20*, 2321–2329. https://doi.org/10.1097/MIB.0000000000000210.

16. Ma, F., Hughes, T.K., Teles, R.M.B., Andrade, P.R., de Andrade Silva, B.J., Plazyo, O., Tsoi, L.C., Do, T., Wadsworth, M.H., Oulee, A., et al. (2021). The cellular architecture of the antimicrobial response network in human leprosy granulomas. Nat. Immunol. *22*, 839–850. https://doi.org/10.1038/s41590-021-00956-8.

17. Wang, A., Rahman, N.T., McGeary, M.K., Murphy, M., McHenry, A., Peterson, D., Bosenberg, M., Flavell, R.A., King, B., and Damsky, W. (2021). Treatment of granuloma annulare and suppression of proinflammatory cytokine activity with tofacitinib. J. Allergy Clin. Immunol. *147*, 1795–1809. https://doi.org/10.1016/j.jaci.2020.10.012.

18. Drent, M., Crouser, E.D., and Grunewald, J. (2021). Challenges of sarcoidosis and its management. N. Engl. J. Med. *385*, 1018–1032. https://doi.org/10.1056/NEJMra2101555.

19. Grunewald, J., Grutters, J.C., Arkema, E.V., Saketkoo, L.A., Moller, D.R., and Müller-Quernheim, J. (2019). Sarcoidosis. Nat. Rev. Dis. Primers *5*, 45. https://doi.org/10.1038/s41572-019-0096-x.

20. Izbicki, G., Chavko, R., Banauch, G.I., Weiden, M.D., Berger, K.I., Aldrich, T.K., Hall, C., Kelly, K.J., and Prezant, D.J. (2007). World Trade Center "sarcoid-like" granulomatous pulmonary disease in New York City Fire Department rescue workers. Chest *131*, 1414–1423. https://doi.org/10.1378/chest.06-2114.

21. Newman, L.S., Rose, C.S., Bresnitz, E.A., Rossman, M.D., Barnard, J., Frederick, M., Terrin, M.L., Weinberger, S.E., Moller, D.R., McLennan, G., et al. (2004). A case control etiologic study of sarcoidosis: environmental and occupational risk factors. Am. J. Respir. Crit. Care Med. *170*, 1324–1330. https://doi.org/10.1164/rccm.200402-249OC.

22. Greaves, S.A., Ravindran, A., Santos, R.G., Chen, L., Falta, M.T., Wang, Y., Mitchell, A.M., Atif, S.M., Mack, D.G., Tinega, A.N., et al. (2021). CD4+ T cells in the lungs of acute sarcoidosis patients recognize an Aspergillus nidulans epitope. J. Exp. Med. *218*. https://doi.org/10.1084/jem.20210785.

23. Facco, M., Cabrelle, A., Teramo, A., Olivieri, V., Gnoato, M., Teolato, S., Ave, E., Gattazzo, C., Fadini, G.P., Calabrese, F., et al. (2011). Sarcoidosis is a Th1/Th17 multisystem disorder. Thorax *66*, 144–150. https://doi.org/10.1136/thx.2010.140319.

24. Crouser, E.D., Locke, L.W., Julian, M.W., Bicer, S., Sadee, W., White, P., and Schlesinger, L.S. (2021). Phagosome-regulated mTOR signalling during sarcoidosis granuloma biogenesis. Eur. Respir. J. *57*. https://doi.org/10.1183/13993003.02695-2020.

25. Pacheco, Y., Lim, C.X., Weichhart, T., Valeyre, D., Bentaher, A., and Calender, A. (2020). Sarcoidosis and the mTOR, Rac1, and autophagy triad. Trends Immunol. *41*, 286–299. https://doi.org/10.1016/j.it.2020.01.007.

26. Calender, A., Weichhart, T., Valeyre, D., and Pacheco, Y. (2020). Current insights in genetics of sarcoidosis: functional and clinical impacts. J. Clin. Med. *9*, 2633. https://doi.org/10.3390/jcm9082633.

27. Calender, A., Lim, C.X., Weichhart, T., Buisson, A., Besnard, V., Rollat-Farnier, P.A., Bardel, C., Roy, P., Cottin, V., Devouassoux, G., et al. (2019). Exome sequencing and pathogenicity-network analysis of five French families implicate mTOR signalling and autophagy in familial sarcoidosis. Eur. Respir. J. *54*, 10–13. https://doi.org/10.1183/13993003.00430-2019.

28. Moller, D.R., Rybicki, B.A., Hamzeh, N.Y., Montgomery, C.G., Chen, E.S., Drake, W., and Fontenot, A.P. (2017). Genetic, immunologic, and environmental basis of sarcoidosis. Ann. Am. Thorac. Soc. *14*, S429–S436. https://doi.org/10.1513/AnnalsATS.201707-565OT.

29. Baughman, R.P., Scholand, M.B., and Rahaghi, F.F. (2020). Clinical phenotyping: role in treatment decisions in sarcoidosis. Eur. Respir. Rev. *29*, 1–8. https://doi.org/10.1183/16000617.0145-2019.

30. Zheng, Y., Wang, H., Xu, Q., Yan, X., Zhuang, Y., Jiang, H., Meng, F., Xiao, Y., Cai, H., and Dai, J. (2019). Risk factors of relapse in pulmonary sarcoidosis treated with corticosteroids. Clin. Rheumatol. *38*, 1993–1999. https://doi.org/10.1007/s10067-019-04507-3.

31. Reynolds, G., Vegh, P., Fletcher, J., Poyner, E.F.M., Stephenson, E., Goh, I., Botting, R.A., Huang, N., Olabi, B., Dubois, A., et al. (2021). Developmental cell programs are co-opted in inflammatory skin disease. Science *371*. https://doi.org/10.1126/science.aba6500.

32. Saluzzo, S., Pandey, R.V., Gail, L.M., Dingelmaier-Hovorka, R., Kleissl, L., Shaw, L., Reininger, B., Atzmüller, D., Strobl, J., Touzeau-Römer, V., et al. (2021). Delayed antiretroviral therapy in HIV-infected individuals leads to irreversible depletion of skin- and mucosa-resident memory T cells. Immunity *54*, 2842–2858.e5. https://doi.org/10.1016/j.immuni.2021.10.021.

33. Crouser, E.D., Culver, D.A., Knox, K.S., Julian, M.W., Shao, G., Abraham, S., Liyanarachchi, S., Macre, J.E., Wewers, M.D., Gavrilin, M.A., et al. (2009). Gene expression profiling identifies MMP-12 and ADAMDEC1 as potential pathogenic mediators of pulmonary sarcoidosis. Am. J. Respir. Crit. Care Med. *179*, 929–938. https://doi.org/10.1164/rccm.200803-490OC.

34. Rosenbaum, J.T., Choi, D., Wilson, D.J., Grossniklaus, H.E., Harrington, C.A., Sibley, C.H., Dailey, R.A., Ng, J.D., Steele, E.A., Czyz, C.N., et al. (2015). Parallel gene expression changes in sarcoidosis involving the lacrimal gland, orbital tissue, or blood. JAMA Ophthalmol. *133*, 770–777. https://doi.org/10.1001/jamaophthalmol.2015.0726.

35. Lockstone, H.E., Sanderson, S., Kulakova, N., Baban, D., Leonard, A., Kok, W.L., McGowan, S., McMichael, A.J., and Ho, L.P. (2010). Gene set analysis of lung samples provides insight into pathogenesis of progressive, fibrotic pulmonary sarcoidosis. Am. J. Respir. Crit. Care Med. *181*, 1367–1375. https://doi.org/10.1164/rccm.200912-1855OC.

36. Pasparakis, M., Haase, I., and Nestle, F.O. (2014). Mechanisms regulating skin immunity and inflammation. Nat. Rev. Immunol. *14*, 289–301. https://doi.org/10.1038/nri3646.

37. Italiani, P., Mosca, E., Della Camera, G., Melillo, D., Migliorini, P., Milanesi, L., and Boraschi, D. (2020). Profiling the course of resolving vs. persistent inflammation in human monocytes: the role of IL-1 family molecules. Front. Immunol. *11*, 1426. https://doi.org/10.3389/fimmu.2020.01426.

38. Grosso, S., Margollicci, M.A., Bargagli, E., Buccoliero, Q.R., Perrone, A., Galimberti, D., Morgese, G., Balestri, P., and Rottoli, P. (2004). Serum levels of chitotriosidase as a marker of disease activity and clinical stage in sarcoidosis. Scand. J. Clin. Lab. Invest. *64*, 57–62. https://doi.org/10.1080/00365510410004092.

39. Inui, N., Murayama, A., Sasaki, S., Suda, T., Chida, K., Kato, S., and Nakamura, H. (2001). Correlation between 25-hydroxyvitamin D3 1α-hydroxylase gene expression in alveolar macrophages and the activity of sarcoidosis. Am. J. Med. *110*, 687–693. https://doi.org/10.1016/S0002-9343(01)00724-0.

40. Kraaijvanger, R., Janssen Bonás, M., Vorselaars, A.D.M., and Veltkamp, M. (2020). Biomarkers in the diagnosis and prognosis of sarcoidosis: current use and future prospects. Front. Immunol. *11*, 1443. https://doi.org/10.3389/fimmu.2020.01443.

41. Shabani, F., Farasat, A., Mahdavi, M., and Gheibi, N. (2018). Calprotectin (S100A8/S100A9): a key protein between inflammation and cancer. Inflamm. Res. *67*, 801–812. https://doi.org/10.1007/s00011-018-1173-4.

42. Martinez, F.O., and Gordon, S. (2014). The M1 and M2 paradigm of macrophage activation: time for reassessment. F1000Prime Rep. *6*, 13. https://doi.org/10.12703/P6-13.

43. Petrova, V., Annicchiarico-Petruzzelli, M., Melino, G., and Amelio, I. (2018). The hypoxic tumour microenvironment. Oncogenesis *7*, 10. https://doi.org/10.1038/s41389-017-0011-9.

44. Piasentin, N., Milotti, E., and Chignola, R. (2020). The control of acidity in tumor cells: a biophysical model. Sci. Rep. *10*, 13613. https://doi.org/10.1038/s41598-020-70396-1.

45. Jin, M.-Z., and Jin, W.-L. (2020). The updated landscape of tumor microenvironment and drug repurposing. Signal Transduct. Target. Ther. *5*, 166. https://doi.org/10.1038/s41392-020-00280-x.

46. Buffa, F.M., Harris, A.L., West, C.M., and Miller, C.J. (2010). Large meta-analysis of multiple cancers reveals a common, compact and highly prognostic hypoxia metagene. Br. J. Cancer *102*, 428–435. https://doi.org/10.1038/sj.bjc.6605450.

47. Mohan, A., Neequaye, N., Malur, A., Soliman, E., McPeek, M., Leffler, N., Ogburn, D., Tokarz, D.A., Knudson, W., Gharib, S.A., et al. (2020). Matrix metalloproteinase-12 is required for granuloma progression. Front. Immunol. *11*, 553949. https://doi.org/10.3389/fimmu.2020.553949.

48. Fireman, E., Kraiem, Z., Sade, O., Greif, J., and Fireman, Z. (2002). Induced sputum-retrieved matrix metalloproteinase 9 and tissue metalloproteinase inhibitor 1 in granulomatous diseases. Clin. Exp. Immunol. *130*, 331–337. https://doi.org/10.1046/j.1365-2249.2002.t01-1-02001.x.

49. Gronski Jr, T.J., Martin, R.L., Kobayashi, D.K., Walsh, B.C., Holman, M.C., Huber, M., Van Wart, H.E., and Shapiro, S.D. (1997). Hydrolysis of a broad spectrum of extracellular matrix proteins by human macrophage elastase. J. Biol. Chem. *272*, 12189–12194. https://doi.org/10.1074/jbc.272.18.12189.

50. Yagi, M., Miyamoto, T., Sawatani, Y., Iwamoto, K., Hosogane, N., Fujita, N., Morita, K., Ninomiya, K., Suzuki, T., Miyamoto, K., et al. (2005). DC-STAMP is essential for cell-cell fusion in osteoclasts and foreign body giant cells. J. Exp. Med. *202*, 345–351. https://doi.org/10.1084/jem.20050645.

51. Van Maarsseveen, T.C.M.T., Vos, W., and Van Diest, P.J. (2009). Giant cell formation in sarcoidosis: cell fusion or proliferation with non-division? Clin. Exp. Immunol. *155*, 476–486. https://doi.org/10.1111/j.1365-2249.2008.03841.x.

52. Bos, J.D., Zonneveld, I., Das, P.K., Krieg, S.R., van der Loos, C.M., and Kapsenberg, M.L. (1987). The skin immune system (SIS): distribution and immunophenotype of lymphocyte subpopulations in normal human skin. J. Invest. Dermatol. *88*, 569–573. https://doi.org/10.1111/1523-1747.ep12470172.

53. Strobl, J., Pandey, R.V., Krausgruber, T., Bayer, N., Kleissl, L., Reininger, B., Vieyra-Garcia, P., Wolf, P., Jentus, M.M., Mitterbauer, M., et al. (2020). Long-term skin-resident memory T cells proliferate in situ and are involved in human graft-versus-host disease. Sci. Transl. Med. *12*, 1–18. https://doi.org/10.1126/SCITRANSLMED.ABB7028.

54. Co, D.O., Hogan, L.H., Il-Kim, S., and Sandor, M. (2004). T cell contributions to the different phases of granuloma formation. Immunol. Lett. *92*, 135–142. https://doi.org/10.1016/j.imlet.2003.11.023.

55. Drayton, D.L., Ying, X., Lee, J., Lesslauer, W., and Ruddle, N.H. (2003). Ectopic LTαβ directs lymphoid organ neogenesis with concomitant expression of peripheral node addressin and a HEV-restricted sulfotransferase. J. Exp. Med. *197*, 1153–1163. https://doi.org/10.1084/jem.20021761.

56. Wolf, M.J., Seleznik, G.M., Zeller, N., and Heikenwalder, M. (2010). The unexpected role of lymphotoxin β receptor signaling in carcinogenesis: from lymphoid tissue formation to liver and prostate cancer development. Oncogene *29*, 5006–5018. https://doi.org/10.1038/onc.2010.260.

57. Hirota, K., Duarte, J.H., Veldhoen, M., Hornsby, E., Li, Y., Cua, D.J., Ahlfors, H., Wilhelm, C., Tolaini, M., Menzel, U., et al. (2011). Fate mapping of IL-17-producing T cells in inflammatory responses. Nat. Immunol. *12*, 255–263. https://doi.org/10.1038/ni.1993.

58. Moser, T., Akgün, K., Proschmann, U., Sellner, J., and Ziemssen, T. (2020). The role of TH17 cells in multiple sclerosis: therapeutic implications. Autoimmun. Rev. *19*, 102647. https://doi.org/10.1016/j.autrev.2020.102647.

59. Ramstein, J., Broos, C.E., Simpson, L.J., Ansel, K.M., Sun, S.A., Ho, M.E., Woodruff, P.G., Bhakta, N.R., Christian, L., Nguyen, C.P., et al. (2016). IFN-γ-producing T-helper 17.1 cells are increased in sarcoidosis and are more prevalent than T-helper type 1 cells. Am. J. Respir. Crit. Care Med. *193*, 1281–1291. https://doi.org/10.1164/rccm.201507-1499OC.

60. Vukmirovic, M., Yan, X., Gibson, K.F., Gulati, M., Schupp, J.C., Deluliis, G., Adams, T.S., Hu, B., Mihaljinec, A., Woolard, T.N., et al. (2021). Transcriptomics of bronchoalveolar lavage cells identifies new molecular endotypes of sarcoidosis. Eur. Respir. J. *58*, 2002950. https://doi.org/10.1183/13993003.02950-2020.

61. van de Berg, P.J., van Leeuwen, E.M., ten Berge, I.J., and van Lier, R. (2008). Cytotoxic human CD4(+) T cells. Curr. Opin. Immunol. *20*, 339–343. https://doi.org/10.1016/j.coi.2008.03.007.

62. Davidson, S., Coles, M., Thomas, T., Kollias, G., Ludewig, B., Turley, S., Brenner, M., and Buckley, C.D. (2021). Fibroblasts as immune regulators in infection, inflammation and cancer. Nat. Rev. Immunol. *21*, 704–717. https://doi.org/10.1038/s41577-021-00540-z.

63. Pober, J.S., and Sessa, W.C. (2007). Evolving functions of endothelial cells in inflammation. Nat. Rev. Immunol. *7*, 803–815. https://doi.org/10.1038/nri2171.

64. Krausgruber, T., Fortelny, N., Fife-Gernedl, V., Senekowitsch, M., Schuster, L.C., Lercher, A., Nemc, A., Schmidl, C., Rendeiro, A.F., Bergthaler, A., and Bock, C. (2020). Structural cells are key regulators of organ-specific immune responses. Nature *583*, 296–302. https://doi.org/10.1038/s41586-020-2424-4.

65. Kambouchner, M., Pirici, D., Uhl, J.F., Mogoanta, L., Valeyre, D., and Bernaudin, J.F. (2011). Lymphatic and blood microvasculature organisation in pulmonary sarcoid granulomas. Eur. Respir. J. *37*, 835–840. https://doi.org/10.1183/09031936.00086410.

66. West, N.R., Hegazy, A.N., Owens, B.M.J., Bullers, S.J., Linggi, B., Buonocore, S., Coccia, M., Görtz, D., This, S., Stockenhuber, K., et al. (2017). Oncostatin M drives intestinal inflammation and predicts response to tumor necrosis factor–neutralizing therapy in patients with inflammatory bowel disease. Nat. Med. *23*, 579–589. https://doi.org/10.1038/nm.4307.

67. Sahai, E., Astsaturov, I., Cukierman, E., DeNardo, D.G., Egeblad, M., Evans, R.M., Fearon, D., Greten, F.R., Hingorani, S.R., Hunter, T., et al. (2020). A framework for advancing our understanding of cancer-associated fibroblasts. Nat. Rev. Cancer *20*, 174–186. https://doi.org/10.1038/s41568-019-0238-1.

68. Croft, A.P., Campos, J., Jansen, K., Turner, J.D., Marshall, J., Attar, M., Savary, L., Wehmeyer, C., Naylor, A.J., Kemble, S., et al. (2019). Distinct fibroblast subsets drive inflammation and damage in arthritis. Nature *570*, 246–251. https://doi.org/10.1038/s41586-019-1263-7.

69. Smillie, C.S., Biton, M., Ordovas-Montanes, J., Sullivan, K.M., Burgin, G., Graham, D.B., Herbst, R.H., Rogel, N., Slyper, M., Waldman, J., et al. (2019). Intra- and inter-cellular rewiring of the human colon during ulcerative colitis. Cell *178*, 714–730.e22. https://doi.org/10.1016/j.cell.2019.06.029.

70. Kramer, N., Schmöllerl, J., Unger, C., Nivarthi, H., Rudisch, A., Unterleuthner, D., Scherzer, M., Riedl, A., Artaker, M., Crncec, I., et al. (2017). Autocrine WNT2 signaling in fibroblasts promotes colorectal cancer progression. Oncogene *36*, 5460–5472. https://doi.org/10.1038/onc.2017.144.

71. Liu, B., Pan, S., Liu, J., and Kong, C. (2021). Cancer-associated fibroblasts and the related Runt-related transcription factor 2 (RUNX2) promote bladder cancer progression. Gene *775*, 145451. https://doi.org/10.1016/j.gene.2021.145451.

72. Wohlfahrt, T., Rauber, S., Uebe, S., Luber, M., Soare, A., Ekici, A., Weber, S., Matei, A.E., Chen, C.W., Maier, C., et al. (2019). PU.1 controls fibroblast polarization and tissue fibrosis. Nature *566*, 344–349. https://doi.org/10.1038/s41586-019-0896-x.

73. Rosa, F.F., Pires, C.F., Kurochkin, I., Ferreira, A.G., Gomes, A.M., Palma, L.G., Shaiv, K., Solanas, L., Azenha, C., Papatsenko, D., et al. (2018). Direct reprogramming of fibroblasts into antigen-presenting dendritic cells. Sci. Immunol. *3*, eaau4292. https://doi.org/10.1126/sciimmunol.aau4292.

74. Krausgruber, T., Blazek, K., Smallie, T., Alzabin, S., Lockstone, H., Sahgal, N., Hussell, T., Feldmann, M., and Udalova, I.A. (2011). IRF5 promotes inflammatory macrophage polarization and TH1-TH17 responses. Nat. Immunol. *12*, 231–238. https://doi.org/10.1038/ni.1990.

75. Sautès-Fridman, C., Petitprez, F., Calderaro, J., and Fridman, W.H. (2019). Tertiary lymphoid structures in the era of cancer immunotherapy. Nat. Rev. Cancer *19*, 307–325. https://doi.org/10.1038/s41568-019-0144-6.

76. Armingol, E., Officer, A., Harismendy, O., and Lewis, N.E. (2021). Deciphering cell–cell interactions and communication from gene expression. Nat. Rev. Genet. *22*, 71–88. https://doi.org/10.1038/s41576-020-00292-x.

77. Vondenhoff, M.F., Greuter, M., Goverse, G., Elewaut, D., Dewint, P., Ware, C.F., Hoorweg, K., Kraal, G., and Mebius, R.E. (2009). LTβR signaling induces cytokine expression and up-regulates lymphangiogenic factors in lymph node anlagen. J. Immunol. *182*, 5439–5445. https://doi.org/10.4049/jimmunol.0801165.

78. Fernandes, N.R.J., Reilly, N.S., Schrock, D.C., Hocking, D.C., Oakes, P.W., and Fowell, D.J. (2020). CD4+ T cell interstitial migration controlled by fibronectin in the inflamed skin. Front. Immunol. *11*, 1501. https://doi.org/10.3389/fimmu.2020.01501.

79. Elices, M.J., Osborn, L., Takada, Y., Crouse, C., Luhowskyj, S., Hemler, M.E., and Lobb, R.R. (1990). VCAM-1 on activated endothelium interacts with the leukocyte integrin VLA-4 at a site distinct from the VLA=4/fibronectin binding site. Cell *60*, 577–584.

80. Hur, E.M., Youssef, S., Haws, M.E., Zhang, S.Y., Sobel, R.A., and Steinman, L. (2007). Osteopontin-induced relapse and progression of autoimmune brain disease through enhanced survival of activated T cells. Nat. Immunol. *8*, 74–83.

81. Barreira Da Silva, R., Laird, M.E., Yatim, N., Fiette, L., Ingersoll, M.A., and Albert, M.L. (2015). Dipeptidylpeptidase 4 inhibition enhances lymphocyte trafficking, improving both naturally occurring tumor immunity and immunotherapy. Nat. Immunol. *16*, 850–858. https://doi.org/10.1038/ni.3201.

82. Celada, L.J., Kropski, J.A., Herazo-maya, J.D., Luo, W., Creecy, A., Abad, A.T., Chioma, O.S., Lee, G., Hassell, N.E., Shaginurova, G.I., et al. (2018). PD-1 up-regulation on CD4+ T cells promotes pulmonary fibrosis through STAT3-mediated IL17A and TGF-b1 production. Sci. Transl. Med. *577*, 561–565. 10. https://doi.org/10.1126/scitranslmed.aar8356.

83. Messina, J.L., Fenstermacher, D.A., Eschrich, S., Qu, X., Berglund, A.E., Lloyd, M.C., Schell, M.J., Sondak, V.K., Weber, J.S., and Mulé, J.J. (2012). 12-Chemokine gene signature identifies lymph node-like structures in melanoma: potential for patient selection for immunotherapy? Sci. Rep. *2*, 765. https://doi.org/10.1038/srep00765.

84. Cabrita, R., Lauss, M., Sanna, A., Donia, M., Skaarup Larsen, M., Mitra, S., Johansson, I., Phung, B., Harbst, K., Vallon-Christersson, J., et al. (2020). Tertiary lymphoid structures improve immunotherapy and survival in melanoma. Nature *577*, 561–565. https://doi.org/10.1038/s41586-019-1914-8.

85. Dieu-Nosjean, M.C., Goc, J., Giraldo, N.A., Sautès-Fridman, C., and Fridman, W.H. (2014). Tertiary lymphoid structures in cancer and beyond. Trends Immunol. *35*, 571–580. https://doi.org/10.1016/j.it.2014.09.006.

86. Wculek, S.K., Dunphy, G., Heras-Murillo, I., Mastrangelo, A., and Sancho, D. (2022). Metabolism of tissue macrophages in homeostasis and pathology. Cell. Mol. Immunol. *19*, 384–408. https://doi.org/10.1038/s41423-021-00791-9.

87. Chang, C.-H., Qiu, J., O'Sullivan, D., Buck, M.D., Noguchi, T., Curtis, J.D., Chen, Q., Gindin, M., Gubin, M.M., Van Der Windt, G.J.W., et al. (2015). Metabolic competition in the tumor microenvironment is a driver of cancer progression. Cell *162*, 1229–1241. https://doi.org/10.1016/j.cell.2015.08.016.

88. Plikus, M.V., Wang, X., Sinha, S., Forte, E., Thompson, S.M., Herzog, E.L., Driskell, R.R., Rosenthal, N., Biernaskie, J., and Horsley, V. (2021). Fibroblasts: origins, definitions, and functions in health and disease. Cell *184*, 3852–3872. https://doi.org/10.1016/j.cell.2021.06.024.

89. Clay, H., Davis, J.M., Beery, D., Huttenlocher, A., Lyons, S.E., and Ramakrishnan, L. (2007). Dichotomous role of the macrophage in early Mycobacterium marinum infection of the zebrafish. Cell Host Microbe *2*, 29–39. https://doi.org/10.1016/j.chom.2007.06.004.

90. Ahidjo, B.A., Maiga, M.C., Ihms, E.A., Maiga, M., Ordonez, A.A., Cheung, L.S., Beck, S., Andrade, B.B., Jain, S., and Bishai, W.R. (2016). The antifibrotic drug pirfenidone promotes pulmonary cavitation and drug resistance in a mouse model of chronic tuberculosis. JCI Insight *1*, e86017. https://doi.org/10.1172/jci.insight.86017.

91. Stuart, T., Butler, A., Hoffman, P., Hafemeister, C., Papalexi, E., Mauck, W.M., Hao, Y., Stoeckius, M., Smibert, P., and Satija, R. (2019). Comprehensive integration of single-cell data. Cell *177*, 1888–1902.e21. https://doi.org/10.1016/j.cell.2019.05.031.

92. Wolf, F.A., Angerer, P., and Theis, F.J. (2018). SCANPY: large-scale single-cell gene expression data analysis. Genome Biol. *19*, 15. https://doi.org/10.1186/s13059-017-1382-0.

93. Lopez, R., Regier, J., Cole, M.B., Jordan, M.I., and Yosef, N. (2018). Deep generative modeling for single-cell transcriptomics. Nat. Methods *15*, 1053–1058. https://doi.org/10.1038/s41592-018-0229-2.

94. Ritchie, M.E., Phipson, B., Wu, D., Hu, Y., Law, C.W., Shi, W., and Smyth, G.K. (2015). limma powers differential expression analyses for RNA-sequencing and microarray studies. Nucleic Acids Res. *43*, e47. https://doi.org/10.1093/nar/gkv007.

95. Hafemeister, C., and Satija, R. (2019). Normalization and variance stabilization of single-cell RNA-seq data using regularized negative binomial regression. Genome Biol. *20*, 296. https://doi.org/10.1186/s13059-019-1874-1.

96. Efremova, M., Vento-Tormo, M., Teichmann, S.A., and Vento-Tormo, R. (2020). CellPhoneDB: inferring cell–cell communication from combined expression of multi-subunit ligand–receptor complexes. Nat. Protoc. *15*, 1484–1506. https://doi.org/10.1038/s41596-020-0292-x.

97. Aibar, S., González-Blas, C.B., Moerman, T., Huynh-Thu, V.A., Imrichova, H., Hulselmans, G., Rambow, F., Marine, J.C., Geurts, P., Aerts, J., et al. (2017). SCENIC: single-cell regulatory network inference and clustering. Nat. Methods *14*, 1083–1086. https://doi.org/10.1038/nmeth.4463.

98. Van de Sande, B., Flerin, C., Davie, K., De Waegeneer, M., Hulselmans, G., Aibar, S., Seurinck, R., Saelens, W., Cannoodt, R., Rouchon, Q., et al. (2020). A scalable SCENIC workflow for single-cell gene regulatory network analysis. Nat. Protoc. *15*, 2247–2276. https://doi.org/10.1038/s41596-020-0336-2.

99. Brüggen, M.-C., Klein, I., Greinix, H., Bauer, W., Kuzmina, Z., Rabitsch, W., Kalhs, P., Petzelbauer, P., Knobler, R., Stingl, G., and Stary, G. (2014). Diverse T-cell responses characterize the different manifestations of cutaneous graft-versus-host disease. Blood *123*, 290–299. https://doi.org/10.1182/blood-2013-07-514372.

100. Caton, M.L., Smith-Raska, M.R., and Reizis, B. (2007). Notch-RBP-J signaling controls the homeostasis of CD8- dendritic cells in the spleen. J. Exp. Med. *204*, 1653–1664. https://doi.org/10.1084/jem.20062648.

101. Xu, C., Lopez, R., Mehlman, E., Regier, J., Jordan, M.I., and Yosef, N. (2021). Probabilistic harmonization and annotation of single-cell transcriptomics data with deep generative models. Mol. Syst. Biol. *17*, e9620. https://doi.org/10.15252/msb.20209620.

102. McInnes, L., Healy, J., Saul, N., and Großberger, L. (2018). UMAP: uniform manifold approximation and projection. J. Open Source Softw. *3*, 861. https://doi.org/10.21105/joss.00861.

103. Traag, V.A., Waltman, L., and van Eck, N.J. (2019). From Louvain to Leiden: guaranteeing well-connected communities. Sci. Rep. *9*, 5233. https://doi.org/10.1038/s41598-019-41695-z.

104. Subramanian, A., Tamayo, P., Mootha, V.K., Mukherjee, S., Ebert, B.L., Gillette, M.A., Paulovich, A., Pomeroy, S.L., Golub, T.R., Lander, E.S., and Mesirov, J.P. (2005). Gene set enrichment analysis: a knowledge-based approach for interpreting genome-wide expression profiles. Proc. Natl. Acad. Sci. USA *102*, 15545–15550. https://doi.org/10.1073/pnas.0506580102.

105. Andersson, A., Bergenstråhle, J., Asp, M., Bergenstråhle, L., Jurek, A., Fernández Navarro, J., and Lundeberg, J. (2020). Single-cell and spatial transcriptomics enables probabilistic inference of cell type topography. Commun. Biol. *3*, 565. https://doi.org/10.1038/s42003-020-01247-y.

106. Cecchini, M.J., Hosein, K., Howlett, C.J., Joseph, M., and Mura, M. (2018). Comprehensive gene expression profiling identifies distinct and overlapping transcriptional profiles in non-specific interstitial pneumonia and idiopathic pulmonary fibrosis. Respir. Res. *19*, 153. https://doi.org/10.1186/s12931-018-0857-1.

107. Ji, A.L., Rubin, A.J., Thrane, K., Jiang, S., Reynolds, D.L., Meyers, R.M., Guo, M.G., George, B.M., Mollbrink, A., Bergenstråhle, J., et al. (2020). Multimodal analysis of composition and spatial architecture in human squamous cell carcinoma. Cell *182*, 497–514.e22. https://doi.org/10.1016/j.cell.2020.05.039.

STAR★METHODS

KEY RESOURCES TABLE

REAGENT or RESOURCE	SOURCE	IDENTIFIER
Antibodies		
CCL19	R&D systems	Clone: 54909; Cat# MAB361; RRID: AB_2071417
CCR6 – PE	Biolegend	Clone: G034E3; Cat# 353409; RRID: AB_10915968
CCR7 – PE	Biolegend	Clone: G043H7; Cat# 353204; RRID: AB_10913813
CD3 – PE/Dazzle 594	Biolegend	Clone: UCHT1; Cat# 300450; RRID: AB_2563618
CD3e – AF750	R&D systems	Clone: UCHT1; Cat# FAB100S
CD31 – FITC	Biolegend	Clone: WM59; Cat# 303103; RRID: AB_314329
CD38 – PE	BD Bioscience	Clone: HB7; Cat# 347687; RRID: AB_400341
CD45 – PE/CF594	BD Bioscience	Clone: HI30; Cat# 562279; RRID: AB_11154577
CD49d (ITGA4) – FITC	Biolegend	Clone: 9F10; Cat# 304315; RRID: AB_2561758
CD68 – APC	Biolegend	Clone: Y1/82A; Cat# 333810; RRID: AB_2275735
CD90 – FITC	BD Bioscience	Clone: 5E10; Cat# 555595; RRID: AB_395969
CD274 (PD-L1) – AF594	Biolegend	Clone: B7-H1; Cat# 329742; RRID: AB_2650678
CD279 (PD-1) – APC	Biolegend	Clone: EH12.2H7; Cat# 329908; RRID: AB_940475
CHIT1	Atlas Abs	Clone: polyclonal; Cat# HPA010575; RRID: AB_1078512
COL4	Abcam	Clone: polyclonal; Cat# ab6586; RRID: AB_305584
FAP (Fibroblast activation protein)	Helmut Dolznig Lab	Clone: F19
SPP1 (Osteopontin)	Thermofisher	Clone: 7C5H12; Cat# MA5-17180; RRID:AB_2538651
Fixable viability dye – eFluor780	eBioscience	Cat#: 65-0865-14
Fluorescein/Oregon green – AF488	Invitrogen	Cat# A11096; RRID: AB_221558
Mouse IgG – AF488	Invitrogen	Cat# A11001; RRID: AB_2534069
Mouse IgG – AF750	Invitrogen	Cat# A21037; RRID: AB_1500644
Mouse IgG – AF647	Invitrogen	Cat# A21240; RRID: AB_141658
Rabbit IgG - PE	Invitrogen	Cat# P2771MP; RRID: AB_221651
TotalSeq-A0252 anti-human Hashtag 2 Antibody	Biolegend	Clone: LNH-94;2M2; Cat# 394603; RRID: AB_2750016
TotalSeq-A0253 anti-human Hashtag 3 Antibody	Biolegend	Clone: LNH-94;2M2; Cat# 394605; RRID: AB_2750017
TotalSeq-A0254 anti-human Hashtag 4 Antibody	Biolegend	Clone: LNH-94;2M2; Cat# 394607; RRID: AB_2750018
Biological samples		
6mm skin biopsy from patient lesional and non-lesional areas	Medical University of Vienna, Department of Dermatology	N/A
OCT embedded biopsy patient lesional and non-lesional areas	Medical University of Vienna, Department of Dermatology	N/A
Chemicals, peptides, and recombinant proteins		
Collagenase IV	Thermo Fisher Scientific	Cat#: 17104019
DNAse I, RNAse free	Thermo Fisher Scientific	Cat#: EN0521
4¢,6-Diamidine-2¢-phenylindole dihydrochloride (DAPI)	Merk	Cat#: 10236276001
PermaFluor	Thermo Fisher Scientific	Cat#: TA-030-FM
Hematoxylin	Dako	Cat# CS700
Eosin	Dako	Cat# CS701
Bluing buffer	Dako	Cat# CS702
MMP12 inhibitor FPA-014	Foresee Pharmaceuticals	N/A

(*Continued on next page*)

Continued

REAGENT or RESOURCE	SOURCE	IDENTIFIER
Critical commercial assays		
Chromium Single Cell 3' GEM, Library & Gel Bead Kit v3	10x Genomics	Cat# 1000075
Chromium Next GEM Single Cell 3' GEM, Library & Gel Bead Kit v3.1	10x Genomics	Cat# 1000121
Chromium Next GEM Single Cell 3' Kit v3.1 (Dual Index)	10x Genomics	Cat# 1000268
Chromium Single Cell B Chip Kit	10x Genomics	Cat# 1000153
Chromium Next GEM Chip G Kit	10x Genomics	Cat# 1000120
Chromium i7 Multiplex Kit,	10x Genomics	Cat# 120262
Single Index Kit T Set A,	10x Genomics	Cat# 1000213
Dual Index Kit TT Set A	10x Genomics	Cat# 1000215
Visium Spatial Gene Expression Slide & Reagent Kit	10x Genomics	Cat# 1000184
Visium Accessory Kit	10x Genomics	Cat# 1000194
Deposited data		
De-identified patient scRNA-seq and spatial transcriptomics data	This paper	GEO Accession: GSE192461
Raw scRNA-seq and spatial transcriptomics data	This paper	EGA Accession: EGAS00001006970
Raw microscopy images	This paper	Zenodo archive: https://doi.org/10.5281/zenodo.7584110
Experimental models: Organisms/strains		
Mouse: $TSC2^{fl/fl}$CD11c Cre^{+}	Weichhart Lab, Medical University of Vienna	JAX: 027458 JAX: 008068
Oligonucleotides		
HTO cDNA PCR additive primer: v2: GTGACTGGAGTTCAGACGTGTGC TCTTCCGAT*C*T	Biolegend: https://www.biolegend.com/en-us/protocols/totalseq-a-antibodies-and-cell-hashing-with-10x-single-cell-3-reagent-kit-v3-3-1-protocol	HTO_add_v2
SI-PCR primer: AATGATACGGCGA CCACCGAGATCTACACTCTTTCCC TACACGACGC*T*C	Biolegend: https://www.biolegend.com/en-us/protocols/totalseq-a-antibodies-and-cell-hashing-with-10x-single-cell-3-reagent-kit-v3-3-1-protocol	10x_SIPCR
10x_D701: CAAGCAGAAGACGGC ATACGAGATCGAGTAAT GTGACT GGAGTTCAGACGTGT*G*C	Biolegend: https://www.biolegend.com/en-us/protocols/totalseq-a-antibodies-and-cell-hashing-with-10x-single-cell-3-reagent-kit-v3-3-1-protocol	10x_D701
10x_D702: CAAGCAGAAGACGGC ATACGAGATTCTCCGGAGTGACT GGAGTTCAGACGTGT*G*C	Biolegend: https://www.biolegend.com/en-us/protocols/totalseq-a-antibodies-and-cell-hashing-with-10x-single-cell-3-reagent-kit-v3-3-1-protocol	10x_D702
10x_D703: CAAGCAGAAGACGGC ATACGAGATAATGAGCGGTGACT GGAGTTCAGACGTGT*G*C	Biolegend: https://www.biolegend.com/en-us/protocols/totalseq-a-antibodies-and-cell-hashing-with-10x-single-cell-3-reagent-kit-v3-3-1-protocol	10x_D703
10x_D704: CAAGCAGAAGACGGC ATACGAGATGGAATCTCGTGACT GGAGTTCAGACGTGT*G*C	Biolegend: https://www.biolegend.com/en-us/protocols/totalseq-a-antibodies-and-cell-hashing-with-10x-single-cell-3-reagent-kit-v3-3-1-protocol	10x_D704
Software and algorithms		
Graphpad Prism v9.3.1	GraphPad Software	https://www.graphpad.com/scientific-software/prism/
Inkscape v1.2	Inkscape	https://inkscape.org

(*Continued on next page*)

Continued

REAGENT or RESOURCE	SOURCE	IDENTIFIER
TissueQuest Software v6	Tissue Gnostics	https://tissuegnostics.com/products/single-cell-analysis/tissuequest
Seurat v3	Stuart et al.[91]	https://github.com/satijalab/seurat
SCANPY v1.8.1	Wolf et al.[92]	https://github.com/scverse/scanpy/tree/2e98705347ea484c36caa9ba10de1987b09081bf
scVI v0.9.0	Lopez et al.[93]	https://docs.scvi-tools.org/en/0.15.1/user_guide/models/scvi.html
Limma v3.46.0	Ritchie et al.[94]	https://bioconductor.org/packages/release/bioc/html/limma.html
Sctransform v0.3.2	Hafemeister and Satija[95]	https://github.com/satijalab/sctransform
CellPhoneDB v2.1.7	Efremova et al.[96]	https://github.com/ventolab/CellphoneDB
SCENIC v1.1.2	Aibar et al.[97]	https://github.com/aertslab/SCENIC
pySCENIC v0.11.2	Van de Sande et al.[98]	https://github.com/aertslab/pySCENIC
Cell Ranger v3.0.2	10x Genomics	https://support.10xgenomics.com/single-cell-gene-expression/software/overview/welcome
Space Ranger v1.2.0	10x Genomics	https://support.10xgenomics.com/spatial-gene-expression/software/overview/welcome
Loupe Browser v5.0.0	10x Genomics	https://www.10xgenomics.com/products/loupe-browser/downloads
Source code	This paper	Zenodo archive: https://doi.org/10.5281/zenodo.7523056
Other		
Digital thickness gauge	Käfer	FD 50/25
Resource website for the sarcoidosis publication	This paper	http://granuloma-map.bocklab.org

RESOURCE AVAILABILITY

Lead contact

Further information and requests for resources and reagents should be directed to and will be fulfilled by the lead contact, Georg Stary (georg.stary@meduniwien.ac.at).

Materials availability

This study did not generate new unique reagents.

Data and code availability

- The scRNA-seq and spatial transcriptomics data have been deposited in GEO in the form of count matrices that are not personally identifiable and are publicly available. The accession number is listed in the Key Resources Table. An overview of all data is provided by the following website: http://granuloma-map.bocklab.org. The raw scRNA-seq and spatial transcriptomics data will be available from the European Genome-phenome Archive as controlled access. The accession number is listed in the Key Resources Table. To access the raw sequencing data, interested researchers need to apply via a data access committee and commit themselves not to pursue re-identification of the study participants, in compliance with legal, regulatory, and ethical requirements. The raw imaging data have been deposited in Zenodo and are publicly available. The DOI is listed in the Key Resources Table.
- A stable long-term archive of the source code underlying the presented analyses has been deposited in Zenodo and is publicly available. The DOI is listed in the Key Resources Table. The source code is also available from the following website: http://granuloma-map.bocklab.org.
- Any additional information required to reanalyze the data reported in this paper is available from the lead contact upon request.

METHOD DETAILS

Patients and sample collection

This study included patients diagnosed with active chronic cutaneous sarcoidosis who enrolled in an interventional clinical trial at the Medical University of Vienna (EudraCT Number: 2017-004930-27). All patients participated voluntarily and provided written informed

consent. The research complies with national law and has been approved by the ethics commission of the Medical University of Vienna (ECS 2242/2017). Only samples collected at baseline of the clinical trial (i.e., before any experimental intervention) were used in this study. Samples were taken as 6 mm punch biopsies of lesional and non-lesional skin (the latter with no signs of inflammation). Sarcoidosis was histologically and clinically confirmed by trained dermatologists. Fresh biopsies were divided into two parts and immediately digested according to a collagenase IV skin digestion protocol[99] to generate single-cell suspensions, or embedded in optimal cutting temperature (OCT) compound for experiments requiring cryosectioning. Patient characteristics, study inclusion criteria, and sample properties are documented in Table S1.

Flow cytometry and cell sorting

Single-cell suspensions of lesional and non-lesional skin were stained for surface markers as previously described[31] and viable CD45$^+$ and CD45- cells were sort-purified on a BD Biosciences FACS Aria III using FACS Diva software. Detailed information on the antibodies used in this study (clone, dilution, etc.) are providedin the Key Resources Table.

Single-cell RNA sequencing

Single-cell RNA-seq (scRNA-seq) libraries were generated using the Chromium Controller and the Next GEM Single Cell 3' Reagent Kit (v3 or v3.1, 10x Genomics) according to the manufacturer's instructions. Single cell suspensions obtained from lesional and non-lesional skin were incubated with commercially available DNA-labeled antibodies (TotalSeq-A, Biolegend) together with an antibody against CD45 and a cell viability dye at 4 °C for 30 min. Following incubation, cell suspensions were washed three times with PBS containing BSA. After the final wash, cell suspensions were resuspended in PBS containing BSA and a viability dye for discrimination between live and dead cells. Next, 10,000 viable CD45+ cells and 10,000 viable CD45- cells were sort-purified from lesional and non-lesional skin. Those four cell fractions were pooled for processing as a single sample according to the manufacturer's protocol, while the antibody-linked barcodes enabled sample-specific demultiplexing of the sequencing data. Libraries were sequenced by the Biomedical Sequencing Facility at the CeMM Research Center for Molecular Medicine of the Austrian Academy of Sciences, using the Illumina HiSeq 3000/4000 platform, except for two libraries that were sequenced on the NovaSeq 6000 platform: (P12_V06 and P13_V06). Raw sequencing data were pre-processed and demultiplexed using Cell Ranger (v3.0.2, 10x Genomics). Sequencing statistics are provided in Table S2.

Spatial transcriptomics

Spatial transcriptomic libraries were generated using the Visium Spatial Gene Expression Reagent Kit (10x Genomics). Skin biopsies were embedded in OCT and stored as sectioning blocks at -80 °C until further processing. Before undertaking the full protocol, a tissue optimization experiment was performed with the Visium Spatial Tissue Optimization (10x Genomics) using cryosections of patient skin biopsies with imaging of fluorescence signal, which identified 18 minutes as the optimal permeabilization time. Skin biopsies from 12 patients with sarcoidosis were then processed for spatial transcriptomics analysis following the manufacturer's instructions. Samples were cut in a precooled cryostat at 10 μM thickness and placed onto the designated capture area of the slide. Next, the slides underwent fixation and H&E staining with immediate imaging on an Olympus IX83 live imaging microscope equipped with a Hamamatsu ORCA-Flash4.0 sCMOS camera using tenfold magnification. This was followed by permeabilization for 18 minutes, reverse transcription, and second strand synthesis, all performed on the slide. An aliquot of the cDNA was used to determine the optimal number of cDNA amplification cycles (i.e., the Cq value of an individual sample at 25% of peak fluorescence intensity) using KAPA SYBR FAST qPCR kit (KAPA Biosystems). Libraries were prepared according to the manufacturer's instructions and sequenced by the Biomedical Sequencing Facility at the CeMM Research Center for Molecular Medicine of the Austrian Academy of Sciences, using the Illumina NovaSeq 6000 platform. Raw sequencing data were preprocessed and demultiplexed using Space Ranger (v1.2.0, 10x Genomics). Sequencing statistics are provided in Table S2.

Immunofluorescence protein staining of patient samples

Multicolor immunofluorescence protein staining for cell surface markers was performed on 7 μm cryosections. One part of 6 mm punch biopsy samples of human skin was embedded in Tissue-Plus OCT Compound (Scigen Scientific), deep-frozen in liquid nitrogen, and stored at -80 °C until further processing. OCT-embedded tissue samples from patients (Table S2) were cut into 7 μm sections and mounted on SuperFrost PLUS adhesion slides (Thermo Fisher Scientific). Air dried sections were fixed in acetone (Sigma Aldrich) for 10 min and stored at -20 °C until immunofluorescence protein staining and imaging, done as previously described.[99] Slides were scanned using a Z1 Axio Observer microscope equipped with an LD Plan-Neofluar 20x/0.4 objective (Zeiss) and a TissueFAXS imaging system, and analyzed using TissueQuest software (Tissue Gnostics). Epidermis, blood vessels, and apocrine glands were excluded from the analysis. The dermal compartment was divided into granuloma areas and areas containing no granulomas. Analyses were performed on two representative sections as replicates. Statistical analysis of the imaging data was performed using GraphPad Prism (v9.0). To determine statistically significant differences between two matched groups, we used paired two-tailed Student's t-test.

Sarcoidosis mouse model and MMP12 treatment

TSC2$^{fl/fl}$ mice[12] were crossed with mice expressing Cre recombinase under the control of the CD11c promoter to delete the *TSC2* gene specifically in CD11c expressing cells.[100] The resulting *TSC2*$^{fl/fl}$ CD11c Cre$^+$ mice developed spontaneous sarcoid-like

granulomas and swelling of the paws and the tail.[12] The mice were age-matched across five experimental batches and had access to food and water ad libitum. To assess the effect of MMP12 treatment, 20 to 24 weeks old female $TSC2^{fl/fl}$ CD11c Cre^{+} mice were orally gavaged with the MMP12 inhibitor FPA-014 (Foresee Pharmaceuticals) at a low dose of 10 mg/kg (n=7), a high dose of 30 mg/kg (n=11), or with vehicle control (n=13, distilled water), every day for four weeks. Moreover, $TSC2^{fl/fl}$ CD11c Cre^{-} mice (n=6) were used as genetic controls. After four weeks of treatment, the mice were sacrificed and the thickness of the front paw, hind paw, and tail were measured using a digital thickness gauge (Käfer FD 50/25) as an external indication of granuloma lesion severity. An average of five consecutive measurements was taken for the left front paw, left hind paw, and tail of each mouse. Mice were bred and maintained at the Medical University of Vienna in accordance with institutional policies and federal guidelines. These experiments were approved by the Austrian ethics committee for animal experiments (GZ.BMBWF 2020-0.547.514).

Preprocessing and analysis of scRNA-seq data

The scRNA-seq data were processed using Cell Ranger (v3.0.2, 10x Genomics). Raw sequencing data were demultiplexed and converted to FASTQ format using the Cell Ranger command *mkfastq*. FASTQ files were aligned to the human reference genome assembly GRCh38, and count matrices were generated per sample using genome annotation v93 and the Cell Ranger command *count*. Each cell was annotated with the sample origin (lesional or non-lesional skin) as part of sample demultiplexing. The demultiplexing was based on a Gaussian mixture model fitted to hashtag antibody counts, inferring the probability that a given antibody read count derives from background or constitutes positive signal.

For each sample, quality control was performed with thresholds for the following metrics: (i) minimum number of detected genes, (ii) maximum fraction of mitochondrial reads, and (iii) maximum fraction of ribosomal genes. The thresholds were determined for each sample following manual inspection of the distribution of each quality control metric (Table S2). Cells that did not meet these criteria were discarded. The gene count matrices of the remaining cells were aggregated using the Cell Ranger command *aggr* without depth normalization.

Automated cell type assignment was performed with the *scANVI*[101] method for label transfer, using a recently published healthy skin dataset[31] as the reference. To reduce the number of features for both the reference and query datasets, we first selected for the genes expressed in more than 10% of the cells or in at least five cells with an average count greater than 1.5; we then used the *highly_variable_genes* function of *Scanpy* (v1.8.1)[92] with the *Seurat* method (v3)[91] to identify the top 3000 most variable genes in either dataset. To further refine the cell type assignment, we performed a subsequent *scANVI* analysis on all cells labeled ''Th'' and ''Melanocytes,'' as manual inspection indicated greater diversity within these cell subsets than reflected by the original labels from the reference dataset.

To integrate the individual samples and to perform dimensionality reduction and clustering, we used the *scVI* method (v 0.9.0)[93] and the same feature selection strategy as described above for the *scANVI* method. To generate a neighbor graph and a 2D visualization of the latent space, the UMAP[102] method was run on the latent space inferred by *scVI*. Clustering was performed using the Leiden method[103] on the UMAP graph (clustering resolution 0.7). The same analysis was performed separately and independently for all myeloid cells (clustering resolution 0.15 and 0.5), lymphoid cells (clustering resolution 0.3), and fibroblasts (clustering resolution 0.15), in order to enable cell subset identification. To integrate a previously published scRNA-seq dataset for healthy skin,[32] we used the *scVI* method and the top 3000 most variable genes across both datasets.

Cell type labels were then assigned to each cluster based on the *scANVI* automatic annotation. Marker genes were detected by differential gene expression analysis between an individual cell cluster and all the other cells. We used *limma* (v3.46.0)[94] on counts normalized using the *sctransform* method (v0.3.2),[95] limited to the top 2000 most variable genes and controlling for quality metrics (ribosomal fraction, mitochondrial fraction) as well as the experimental batch that each sample was part of. The identified marker genes allowed for manual validation and improvement of the automatic assignments, especially for the lymphoid compartment where high heterogeneity was observed.

Differential gene expression analysis was performed by comparing the granuloma-associated cluster with the homeostatic cluster for each cell type except for the endothelial cells (where we compared lesional and non-lesional cells because endothelial cells were not split into two clusters by the Leiden algorithm). The differential expression analysis was implemented using *limma* applied to gene counts normalized using the *sctransform* method (v0.3.2),[95] controlling for quality metrics (ribosomal fraction, mitochondrial fraction) as well as the experimental batch that each sample was part of. We included only those genes that were expressed in at least 25% of cells or had an average normalized log count of at least two (the average was computed considering only those cells were the gene was expressed).

For visual inspection and validation, the heatmaps and gene expression plots were generated using the expression data normalized on total counts per cell and standardized by gene expression mean and variance across cells. The heatmaps were clustered using hierarchical clustering on differential genes that were manually selected based on biological interpretability, while also presenting with an adjusted p-value lower than 10^{-50} and a log-fold-change greater than 0.1. A complete list of all differentially expressed genes is provided in Table S3. Top differential genes were defined as those with an adjusted p-value lower than 10^{-50}, a log-fold-change greater than 0.3, and detection of the gene in the top 5% of either fold-change or p-value. For all the genes that were tested for differential expression (ranked by fold change), we ran gene set enrichment analysis[104] against the following databases: "MSigDB ontology (C5), hallmark (H), and curated (C2)." A list of enriched pathways is provided in Table S4.

To dissect the cell-type-specific crosstalk of immune cells and structural cells, we quantified the enrichment of known ligand-receptor pairs using CellPhoneDB (v2.1.7)[96] applied to the gene counts transformed with the *sctransform* method (v0.3.2).[95] A full list of cell-cell interactions identified with CellphoneDB is provided in Table S5.

To reconstruct gene-regulatory networks we used the SCENIC software (v1.1.2).[97] SCENIC identifies regulons (i.e., transcription factors and their target genes) and assesses the activity of these discovered regulons in individual cells. These cellular activity patterns are then used to find clusters of similar cells. Regulon analysis was ran using *pySCENIC* (v0.11.2)[98] on the SCT-normalized counts, batch-corrected using *ComBat*, and differential regulon activity was detected using a t-test between groups.

Preprocessing and analysis of spatial transcriptomics data

Raw base calls from the sequencer were demultiplexed and converted to FASTQ format using the Cell Ranger (v3.0.2, 10x Genomics) command *mkfastq*. FASTQ files were aligned to the human reference genome assembly GRCh38 and a count matrix was generated based on genome annotation v32 using the Space Ranger (v1.2.0, 10x Genomics) command *count*.

For each spatial transcriptomics sample, quality control was performed by manually selecting spatial transcriptomics spots that appeared intact and did not show signs of folded tissue, using the Loupe Browser (v5.0.0, 10x Genomics). For those spots, we performed additional quality control based on inspection of the (i) number of detected genes, (ii) fraction of mitochondrial reads, and (iii) fraction of ribosomal. All the selected spots passed these criteria, and no additional filtering was needed (Table S2). The gene count matrices of the selected spatial transcriptomic spots were aggregated using the Space Ranger command *aggr* without depth normalization.

To integrate the various samples and to perform dimensionality reduction and clustering, we used the *scVI* method[93] (v0.9.0; model trained with 2000 epochs). To reduce the number of genes to compare, we first selected those genes that were expressed in more than 10% of spots or that were expressed in at least 5 spots with an average count greater than 1.5. Out of these genes we selected only those that were among the top 2000 most variable genes as identified by the *highly_variable_genes* function in *Scanpy* (v1.8.1)[92] with the *Seurat* method (v3).[91] As described above for the scRNA-seq data, the UMAP method was run on the latent space from *scVI* (n neighbours = 15, min_dist = 0.1), and clustering was performed using the Leiden method (resolution = 0.15) on the UMAP graph.

To infer the composition of the spatial transcriptomic spots, we used the *stereoscope* method[105] in the *scVI* suite, with the cluster labels and the tissue labels. We removed rare cell types and corrected for possible over-representation of rare immune cell subsets in the scRNA-seq dataset by selecting only those cells that belong to cell types with a frequency higher than 10% in the immune cell compartment and higher than 2% in the structural cell compartment. We selected the top 6500 most variable genes in the scRNA-seq dataset when transferring cluster labels and the top 4000 variable genes when transferring lesional and non-lesional skin labels.

To obtain normalized data for the visualizations, we trained an *scVI* model individually for each sample using all genes. The literature-derived gene signatures were extracted from the following tables and figures of the original publications: hypoxia signature[46]: Table S5; 12-chemokine signature[83]: Figure 2B; TLS-melanoma signature[84]: Figure 3A; TLS-hallmark signature as reviewed in[85]; lung granuloma[33]: Figure 3; Table 3; orbital adipose tissue granuloma[34]: Table 2; lacrimal gland tissue granuloma[34]: Table 3; progressive fibrotic lung tissue granuloma[35]: Figure 1; IPF signature[106]: Table S1; NSIP signature[106]: Table S3. A list of included genes for each gene signature is provided as Table S6. Expression levels of gene signatures (the granuloma tissue signatures in Figure S2E, hypoxia signature in Figure S3H, 12-chemokine signature in Figure 7B, TLS signatures in Figures S7B and S7C, fibrotic IPF and inflammatory NSIP signatures in Figure S7G) in the spatial transcriptomics data were calculated as the average z-score of the normalized gene expression of all genes in the respective signature. The contributions of individual genes to a given signature were calculated as the average z-score of normalized gene expression across all spatial transcriptomics spots in the cluster. For displaying selected ligand-receptor pairs in the spatial transcriptomics data, we used the maximum z-score of normalized gene expression if the interacting partner was a protein complex made from several genes.

The validation of increased co-expression among ligand-receptor interaction partners in the granulomas was inspired by a published method.[107] Based on spatial transcriptomic clusters from Figure 2D, we defined this metric as the difference between means of ligand-receptor average expression distributions in granulomatous dermis (cluster 0) compared to unaffected dermis (cluster 1). We then calculated the null distribution by reshuffling the spot labels in each sample and recalculating the difference in means per area across 10^6 perturbations. The p-value for a given interaction in a given sample was defined as the number of permutations in which the randomized value was higher than the observed value. Afterward, all p-values were adjusted for multiple testing using the Bonferroni method across all interaction pairs and samples. To evaluate if the co-expression patterns were significant across patients, we additionally trained the *scVI* model on all genes and aggregated samples and calculated the average ligand-receptor co-expression values using the normalized data. For each interaction, we performed an unpaired t-test with Bonferroni correction between co-expression values in cluster 0 versus 1 (granulomatous dermis versus unaffected dermis). All statistical comparisons were performed using the *add_stats_annotation* function from the *statannot* package in R (https://doi.org/10.5281/zenodo.6607135).

Statistical analysis of immunofluorescent protein staining

GA-associated cell subsets were localized in lesional sarcoidosis skin cryosections using immunofluorescent protein staining. Acquired images were imported into TissueQuest (v6, TissueGnostics) which identifies cells based on nuclei staining and quantifies cell populations based on the expression of cell surface markers. Image analysis was performed on two representative lesional skin sections as replicates with DAPI staining nuclei of all dermal cells. Lesional skin sections were divided in epidermal and dermal regions and only the dermal regions were included in the final analyses. Apocrine glands were excluded from all analyses to avoid the

high autofluorescent signal associated with these structures. The threshold of a positive signal for each surface or intracellular marker was set manually after comparison to the respective isotype control staining on separate lesional skin sections. For all markers, the same thresholds for the intensity of the fluorescent signal identifying a cell as ''positive'' or ''negative'' were used. We localized dermal macrophages, T cells and fibroblasts using CD68, CD3, and CD90 as cell-type-defining surface markers. Next, granulomas were identified as compact cell structures with a strong positive signal for CD90+ fibroblasts on the outside and a dense composition of CD68+ macrophages, with T cells scattered between macrophages and fibroblasts. The dermal compartment was further subdivided into two groups: the first group comprised dermal regions containing granulomas, and the second group included dermal regions containing no granulomas. These regions were close to each other, and we used the outer fibroblast layer of granulomas as the respective subclassification line. The following parameters were determined for each dermal subgroup: cell count per mm^2, mean intensity of the marker of interest (detailed in the respective figure legends), and relative percentage of the parent population. Statistical analysis was performed using a paired t-test between the two dermal subgroups or an unpaired t-test when comparing the dermal subgroups and patient matched non-lesional skin. The following cell populations were compared between dermal regions containing granulomas and dermal regions containing no granulomas: CD3+CCR6+ T cells, CD68+CHIT1+ macrophages, CD3+PD1+ T cells, and CD68+PDL1+ macrophages. Moreover, CD3+CCR6+ T cells were compared between dermal regions containing granulomas, dermal regions containing no granulomas, and dermal regions of patient matched non-lesional skin. Data are represented as dot plots showing the mean and standard error of the mean, with each dot representing one replicate of one cryosection. Details for the statistical tests used in each experiment can be found in figure legends and the methods section. Statistical significance testing was performed with Graphpad prism (v9.3.1), and p-values were annotated as follows: *$p<0.05$, **$p<0.01$, ***$p<0.001$, ****$p<0.0001$.